

Megacrysts and Associated Xenoliths: Evidence for Migration of Geochemically Enriched Melts in the Upper Mantle beneath Scotland

B. G. J. UPTON^{1*}, R. W. HINTON¹, P. ASPEN¹, A. FINCH² AND
J. W. VALLEY³

¹DEPARTMENT OF GEOLOGY AND GEOPHYSICS, EDINBURGH UNIVERSITY, EDINBURGH EH9 3JW, UK

²FACULTY OF SCIENCE AND COMPUTING, LUTON UNIVERSITY, LUTON LU1 3JU, UK

³DEPARTMENT OF GEOLOGY AND GEOPHYSICS, UNIVERSITY OF WISCONSIN, MADISON, WI 53706, USA

RECEIVED JANUARY 22, 1997; REVISED TYPESCRIPT ACCEPTED DECEMBER 8, 1998

Megacrysts, principally anorthoclase, Fe-rich biotite, clinopyroxene, magnetite, zircon and apatite, occur in alkali basaltic hosts at a number of Scottish localities. These minerals occur, not only as discrete, and composite megacrysts, but also as polycrystalline syenite (anorthoclasite) xenoliths. Composite xenoliths provide evidence that the anorthoclasites may occur as (pegmatitic) veins traversing pyroxenitic wall-rocks which may themselves be localized metasomatized peridotites within the shallow mantle. The anorthoclasites crystallized from highly trace element enriched melts which, in the case of the most geochemically extreme samples, were also peraluminous. Ion microprobe analyses show that the peraluminous (corundum-bearing) anorthoclasites comprise light rare earth element (LREE)-enriched alkali feldspars together with corundum and Nb-rich oxides (ilmenorutile, samarskite, yttrio-niobate and columbite). The high contents of incompatible elements, together with oxygen isotope data, indicate crystallization of these syenitic facies from felsic melts, possibly originating through partial melting of metasomatized mantle lithologies. The aluminous character may be explained in terms of preferential loss of alkalis in fugitive carbonatitic fractions separated from the felsic melts.

KEY WORDS: *anorthoclase; corundum; mantle; megacrysts; Scotland*

INTRODUCTION

This paper describes the paragenesis of enigmatic megacryst assemblages in alkaline basalts which appear to be the crystallization products of salic alkaline magmas within the upper mantle and/or within ultramafic facies in the lowermost crust. The dominant mineral phase is alkali feldspar (mainly anorthoclase) suggesting that the magmas from which they crystallized were trachytic in composition. Mineral composition data suggest that some of the parental magmas were geochemically highly evolved; the most extreme compositions were peraluminous, containing modal corundum.

There are some 70 localities in northern Britain and Ireland at which basaltic magmas have brought up deep-seated xenoliths and megacrysts (Upton *et al.*, 1983; Hunter & Upton, 1987). The host magmas, which ascended through crust varying from Archaean to Proterozoic in age (Menzies & Halliday, 1988), ranged from basanite to olivine nephelinite in composition. In Scotland the localities define a broad swath extending from NE Scotland, around the Hebrides and West Highlands and across the Scottish Midland Valley and Southern Uplands, with the greatest concentration in the Midland Valley (Fig. 1). With the exception of one probable Tertiary-age dyke in the Outer Hebrides, the magmatism is mainly late Carboniferous–Permian age. The mega-

*Corresponding author.

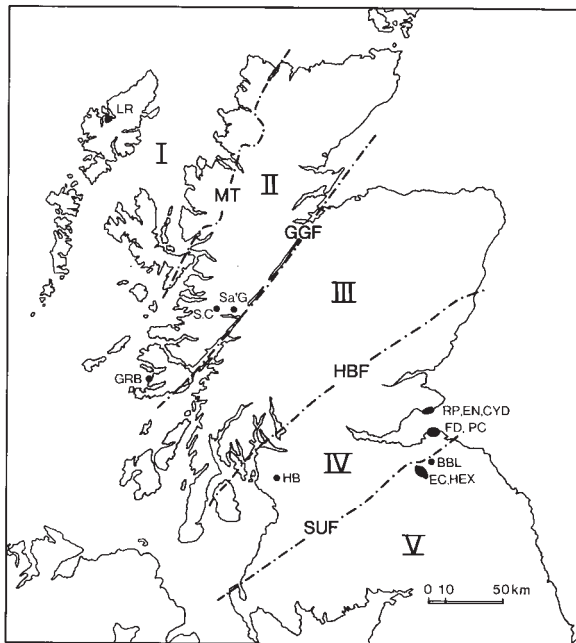


Fig. 1. Map of Scotland showing xenolith-megacryst localities. LR, Loch Roag. SC, Streap Comlaidh. Sa'G, Stobh a'Ghrianain. GRB, Gribun, Isle of Mull. HB, Holmbyre. RP, Ruddon's Point. EN, Elic Ness. CYD, Coalyard Hill. FD, Fidra. PC, Partan Craig. EC, Earnscleugh. BBL, Burn-between-the-Laws. HEX, Hexpath. The principal fault zones are also shown: MT, Moine Thrust; GGF, Great Glen Fault; HBF, Highland Boundary Fault; SUF, Southern Uplands Fault. The localities lie across the main tectonic zones of Scotland, namely: I, Foreland zone; II, Northern Highlands; III, Grampian Highlands; IV, Scottish Midland Valley; V, Southern Uplands.

cryst assemblages considered here are from (a) Loch Roag (Outer Hebrides), (b) The Isle of Mull (Inner Hebrides), (c) localities in the north east of the Scottish Midland Valley and (d) localities in the north east of the Southern Uplands.

Based upon studies of xenoliths and accompanying megacrysts in Scottish alkali basalts, Menzies & Halliday (1988) demonstrated the presence of distinct lithospheric domains, differing in their isotopic characteristics and in their large ion lithophile element (LILE) and light rare earth element (LREE) contents. The commonest xenolith type is spinel lherzolite, probably representing partly recrystallized mantle residues from Precambrian and Palaeozoic melting episodes. Unfoliated, anhydrous ultramafic xenoliths commonly associated with the lherzolitic xenoliths include wehrlites and clinopyroxenites with rare websterites and garnet pyroxenites. Textural evidence suggests that these more calcic and aluminous varieties are younger than the associated lherzolites (Upton *et al.*, 1983) and they are inferred to have been derived from stockworks of sheets within the upper lithospheric mantle (see Irving, 1980). Some of the wehrlites and pyroxenites, which have textures suggesting a magmatic origin, may

have been side-wall cumulates in shallow mantle conduits, as envisaged by, for example, Irving (1980) and Duda & Schmincke (1985), disrupted and transported by ascending magma pulses.

Hydrous ultramafic xenoliths, mainly pargasite and/or biotite-bearing wehrlites and pyroxenites, are also common and although these generally occur together with anhydrous lherzolitic and wehrlitic-pyroxenitic xenoliths, they are the sole ultramafic category at some localities. With variation in mode, they grade into hornblendites (lherzites) and biotitites (glimmerites). The origin of these hydrous xenoliths is debatable; some may have originated as olivine- or olivine-clinopyroxene-cumulates with intercumulus amphibole, crystallized from alkaline basic magmas (see Chapman, 1976), whereas textures in many others (where amphibole and/or biotite appear to have played a replacive role) suggest a metasomatic origin from an anhydrous protolith involving addition of Fe, Ti, K, P, OH⁻ and a wide range of incompatible elements (Upton *et al.*, 1998). Evidence from the very variable xenolith populations of closely adjacent vents in the east of the Midland Valley suggests that the distribution of the hydrous ultramafic facies in the upper lithospheric mantle of this region may be highly localized (Upton *et al.*, 1984). Menzies & Halliday (1988) thought that some of the pyroxenites could be the products of underplating by basaltic magma at the crust-mantle interface. Whereas this possibility is undeniable, the intimate association of the clinopyroxene-rich xenoliths with mantle peridotites at many of the localities is such as to persuade us that most are from the (shallow) lithospheric mantle. Menzies & Halliday (1988) concluded that the Scottish lithosphere is laterally heterogeneous, containing discrete mantle domains. They ascribed much of this heterogeneity to enrichment of variably depleted mantle protoliths by small melt fractions originating within either the lithosphere or the asthenosphere.

GROUP B MEGACRYSTS AND RELATED XENOLITHS

Many of the Scottish xenolith localities also contain abundant megacrysts. Irving (1984) subdivided the megacrysts in alkaline basalts into two categories: Groups A and B. He suggested that Group A megacrysts (Al-augite, Al-bronzite, olivine, kaersutitic amphibole, pyrope garnet, pleonaste and plagioclase) originate as high-pressure phenocrysts cognate with the basaltic hosts, whereas the Group B megacrysts (including anorthoclase, Ti-mica, Fe-Na salite, apatite, magnetite, ilmenite, zircon, corundum, rutile and sphene) are likely to be 'accidental', derived from the crystalline products of more evolved magmas encountered by the rising basic magmas. The

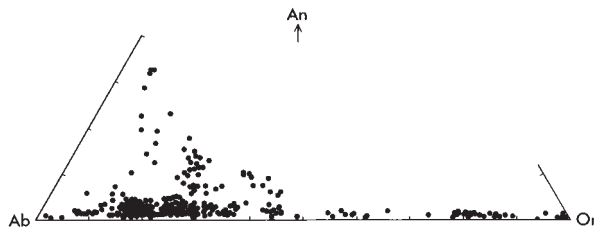


Fig. 2. Compositional range of feldspars in the Group B xenolith-megacryst associations in Scotland. Compilation of data from Aspen *et al.* (1990). Although the total compositional range extends from oligoclase to nearly pure sanidine, the great majority fall in the anorthoclase field.

majority of the megacrysts in the Scottish localities are Group B varieties, although megacrysts of both groups may occur together. Scottish alkali feldspar megacrysts were considered by Aspen *et al.* (1990) to be samples of syenitic residues in the upper mantle. Although the majority are anorthoclases with 10–20 mol % KAlSi_3O_8 they constitute a compositionally broad suite ranging from potassic oligoclase and albite, through both Ca-rich and Ca-poor anorthoclases to nearly pure sanidine (Fig. 2). Compositional ranges for individual localities tend to be distinct (Aspen *et al.*, 1990). Group B megacrysts may represent high-pressure phenocrysts of evolved magmas that were intercepted by, and mixed with larger volumes of more primitive magmas (see Brooks & Printz-lau, 1978; Barton *et al.*, 1982; Duda & Schminke, 1985) or, alternatively, they may have been stripped from the already crystalline products of evolved magmas (see Duda & Schminke, 1985). According to Guo *et al.* (1996a) anorthoclase megacrysts in basalts probably crystallize from benmoreite-like magmas in pegmatitic veins at ~45 km depth.

The Scottish megacryst occurrences are of particular interest because:

(1) composite alkali feldspar megacrysts, grading to syenitic xenoliths and involving mineral species other than alkali feldspar, clearly indicate the paragenetic relationships between different megacryst species;

(2) composite xenoliths demonstrate that these syenitic products can occur, probably as veins, within amphibole pyroxenite or biotite pyroxenite hosts;

(3) the presence of Nb-, Zr-, REE-, Th- and/or U-rich minerals points to extreme concentrations of high field strength elements (HFSE) in some of the melts from which they crystallized (see Guo *et al.*, 1996b; Sutherland *et al.*, 1998);

(4) the most geochemically extreme assemblages also contain magmatic corundum, indicative of crystallization from peraluminous melts.

Apart from zircon and ilmenorutile, other exotic species include yttrio-niobate, samarskite (Aspen *et al.*, 1990;

Hinton & Upton, 1991) and columbite. Small amounts of sulphides (pyrrhotite) are also common.

In the following section, new petrographic and mineral compositional data are presented for the following localities: (1) Loch Roag, Outer Hebrides; (2) Gribun, Isle of Mull, Inner Hebrides; (3) the Ardross fault zone, eastern Midland Valley; (4) Fidra and Partan Craig, eastern Midland Valley; (5) the Southern Uplands (Earnscleugh, Burn-between-the-Laws and Hexpath; Fig. 1).

LOCH ROAG, LEWIS, OUTER HEBRIDES

A small dyke contains a high concentration of xenoliths and megacrysts. Xenoliths of anhydrous spinel peridotite are scarce whereas biotite-bearing peridotites and biotite pyroxenites grading to glimmerites are abundant. REE and Nd and Sr isotopic data for the Loch Roag peridotites, pyroxenites and pyroxene and apatite megacrysts were presented by Menzies & Halliday (1988). Some xenoliths consist of alkali feldspar and corundum (Fig. 3a), with inclusions of zircon, ilmenorutile and the Nb–Th–REE-rich oxide samarskite (Upton *et al.*, 1983; Aspen *et al.*, 1990; Hinton & Upton, 1991). One xenolith (LR247) shows an anorthoclase-rich facies adjacent to a feldspar-free biotite pyroxenite facies and is interpreted as having been part of an anorthoclase vein traversing biotite pyroxenite host rock.

The commonest megacrysts are anorthoclase, biotite and apatite. Less common are corundum (sapphire) megacrysts occurring as smoky blue crystals. Some of the corundum occurs within xenoliths comprising anorthoclase and corundum (Fig. 3a) whereas others appear as discrete euhedral crystals, up to 40 mm long, with pyramidal prismatic habits (Fig. 3b). Other composite megacrysts (or small xenoliths), for example, LR243 and LR245, involve single alkali feldspar crystals (up to 40 mm) containing subhedral, greenish, Na–Fe salite, euhedral brown biotite, magnetite and apatite prisms.

GRIBUN, MULL

An olivine nephelinite dyke, on the island of Mull, is crowded with xenoliths, mainly pargasite-bearing pyroxenites and wehrlites, grading to hornblendites (Upton *et al.*, 1998). The ultramafic xenoliths are tentatively ascribed to a deep crustal or shallow mantle origin. Anhydrous ultramafic xenoliths are notably absent. The amphibole and biotite have been introduced metasomatically after the olivine and pyroxene crystallization. Opaque oxides (magnesian ilmenites and hercynite-rich spinels) are present up to 20% modally and apatite is a conspicuous component in some xenoliths.

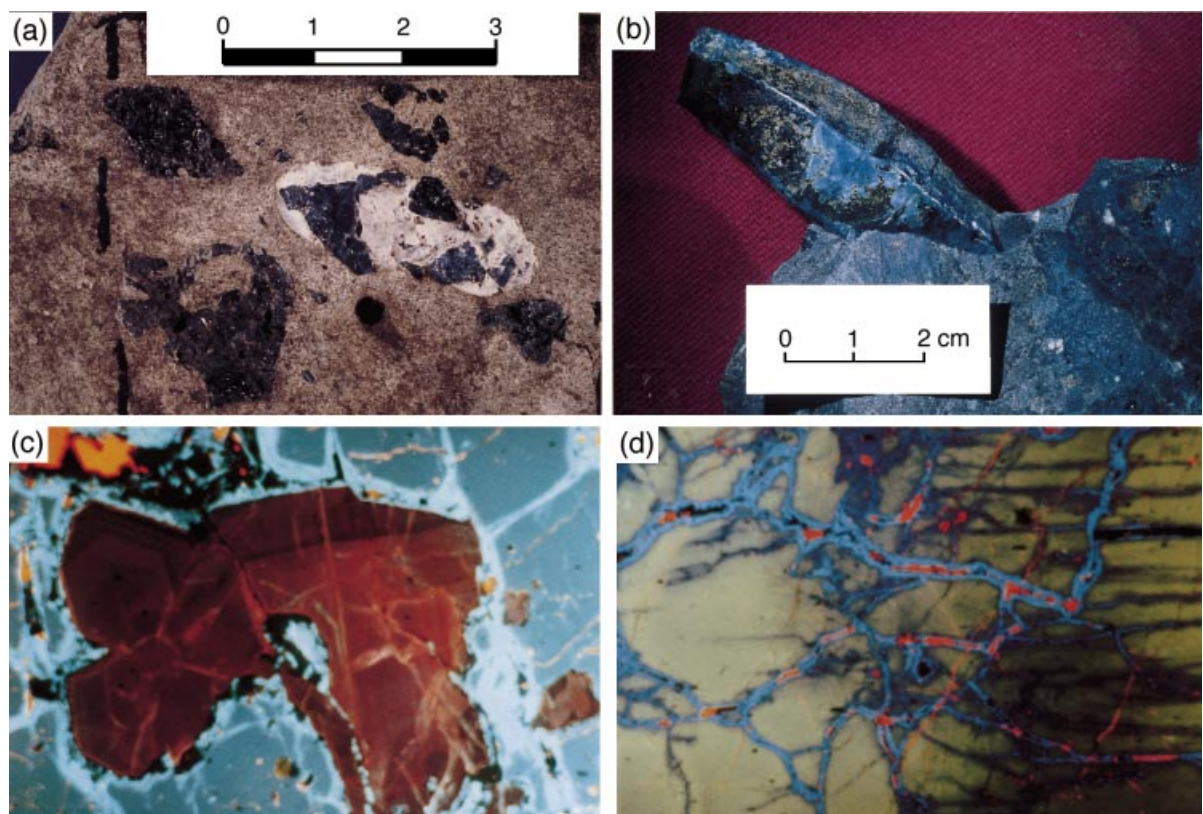


Fig. 3. (a) Corroded megacrysts of corundum and xenolith of corundum–anorthoclase rock in the Loch Roag dyke. (b) A nearly euhedral corundum megacryst, Loch Roag dyke. (c) Cathodoluminescence image of corundum (brown) in BBL24 Burn-between-the-Laws. The zonation and the evidence for resorption and regrowth should be noted. Anorthoclase (dull blue luminescence) with pale blue luminescing veinlets of more potassic feldspar. Calcite shows bright orange luminescence. (d) Cathodoluminescence image of feldspar from the corundum anorthoclase xenolith BBL24, Burn-between-the-Laws. The primary anorthoclase luminesces green. Secondary alteration to more potassic feldspar results in dull blue luminescence and bright blue luminescence. Calcite shows bright orange coloration.

The xenoliths are texturally complex and record various episodes of recrystallization, metasomatism and deformation.

Accompanying megacrysts at Gribun include anorthoclase, clinopyroxene, kaersutite, apatite, magnetite and ilmenite. The relationship between the anorthoclase and the amphibole–pyroxenitic xenoliths is revealed in one critical sample (GRB117). This comprises a pyroxenite composed of colourless diopside ($\text{Ca}_{48.5}\text{Mg}_{41.5}\text{Fe}_{10}$) and pargasite, in sharp planar contact with a coarser layer a few millimetres thick, of pale green clinopyroxene crystals showing an equilibrated texture with 120° intercrystal angles. These green pyroxenes are more iron-rich ($\text{Ca}_{45.5}\text{Mg}_{33.5}\text{Fe}_{21}$), with $\sim 3\%$ Al_2O_3 and $\sim 2\%$ Na_2O (Table 1). The green pyroxenitic layer is relatively rich in opaque oxides, apatite and biotite, and grades (over 1 mm) into coarse, inequigranular anorthoclase syenite (anorthoclase; Upton *et al.*, 1998).

The mean feldspar composition in the anorthoclase is $\text{An}_{8.4}\text{Ab}_{74.8}\text{Or}_{16.8}$ but there is patchy zoning with compositions ranging between $\text{An}_{6.5}\text{Ab}_{73}\text{Or}_{20.5}$ and An_{13}

$\text{Ab}_{78}\text{Or}_9$. This syenitic facies contains subordinate green Na–Fe salite similar to that forming the selvage, together with small crystals of opaque oxide and apatite. Pyrrhotite occurs as blebs around the FeTi oxides.

Sample GRB117 is interpreted as a fragment from a body of amphibole pyroxenite traversed by a younger anorthoclase vein (width > 3 cm) whose walls were lined with pyroxene–oxide–apatite cumulate. The interior of the (supposed) vein probably approximates to an alkali feldspar–ferrosalite cotectic composition. The sample can be compared with the composite xenolith (LR247) from Loch Roag, which shows anorthoclase in contact with a biotite pyroxenite (Aspen *et al.*, 1990). The two instances clearly demonstrate that highly fractionated syenitic facies (veins?) can be hosted by hydrated ultrabasic rocks. Another xenolith (MLL6) comprises a 20 mm fragment consisting of euhedral apatite enclosed by anhedral magnetite and ferrosalite. Although the assemblage is the same as that in the pyroxenitic selvage of GRB117, it is texturally different, implying a stage at which apatite was on the liquidus. Coexisting Ti-magnetite and ilmenite

Table 1: Electron microprobe analyses of relatively iron-rich pyroxenes from Scottish Group B megacrysts and related xenoliths

	1	2	3	4	5	6	7
SiO ₂	49.51	50.21	50.77	47.97	50.76	47.36	55.34
TiO ₂	1.38	1.06	0.54	1.94	0.79	1.51	—
Al ₂ O ₃	6.19	4.47	3.30	6.33	2.90	9.54	4.02
Cr ₂ O ₃	0.25	—	0.03	0.15	0.06	0.01	—
FeO*	13.37	12.52	11.69	10.77	15.16	8.49	7.29
MnO	0.22	0.30	0.51	0.21	0.60	0.19	0.15
MgO	8.41	9.60	10.74	10.05	8.25	9.61	31.89
CaO	17.04	20.17	20.19	20.56	18.15	20.56	0.63
Na ₂ O	3.41	2.16	2.14	2.05	3.31	2.25	—
Sum	99.78	100.49	99.91	99.89	99.88	99.52	99.32
<i>Cations to 6 oxygens</i>							
Si	1.880	1.900	1.926	1.819	1.952	1.780	1.285
Ti	0.040	0.031	0.015	0.055	0.023	0.043	—
Al	0.278	0.200	0.148	0.283	0.123	0.423	0.110
Cr	0.007	—	0.001	0.000	0.002	0.000	—
Fe	0.426	0.396	0.371	0.341	0.488	0.267	0.142
Mn	0.007	0.010	0.016	0.007	0.019	0.006	0.003
Mg	0.477	0.542	0.607	0.568	0.473	0.538	1.104
Ca	0.695	0.818	0.821	0.835	0.748	0.828	0.016
Na	0.252	0.159	0.158	0.150	0.247	0.164	—
Sum	4.062	4.056	4.063	4.059	4.075	4.049	2.660

FeO*, total iron as FeO. 1, Streap Comlaidh; 2, Stob'a Ghriannain; 3, Gribun (GRB 117); 4, Gribun (MLL6); 5, Elie Ness; 6, Loch Roag (LR247); 7, Hexpath (HEX8).

crystals in the Gribun megacryst suite indicate equilibration at temperatures in the range 967–901°C and fO_2 values of –2 to +3 relative to the FMQ (fayalite–magnetite–quartz) buffer (Upton *et al.*, 1998).

THE ARDROSS FAULT ZONE, SCOTTISH MIDLAND VALLEY

A cluster of basaltic vents lies along a fault which is more or less axial to the Midland Valley. Mantle and deep crustal xenoliths in the vents are accompanied by megacrysts of both Groups A and B. The best known of these vents is Elie Ness (Colvine, 1968; Chapman, 1976; Donaldson, 1984), although the Ruddon's Point, Ardross and Coalyard Hill vents have yielded important material. Like the Gribun dyke, the Elie Ness and Ardross vents contain a profusion of hydrated ultramafic xenoliths (Chapman, 1976) but are devoid of anhydrous ultramafic lithologies. In contrast, Ruddon's Point and Coalyard Hill contain abundant spinel lherzolites and (scarcer)

wehrlites as well as biotite- and amphibole-rich pyroxenites. Megacrysts, predominantly of high-temperature alkali feldspars (mainly anorthoclase) also occur at these localities (Aspen *et al.*, 1990). The Elie Ness pyroxenites vary from feldspar-free varieties to those containing albitic feldspar. A xenolith from Coalyard Hill comprises approximately equal proportions of Fe-rich biotite and potassic albite, with accessory zircon, and it is possible that there is a continuum in the protolith between the mafic (host) rocks and the felsic varieties from which the anorthoclase megacrysts were derived.

Small anorthoclase xenoliths are known from Ruddon's Point and Elie Ness; these typically have a simple mineralogy involving anorthoclase with subordinate zircon and chlorite pseudomorphs inferred to be after pyroxene. One small anorthoclase xenolith (EN4) has a primary anorthoclase (An_{2.4}Ab_{81.0}Or_{16.6}) traversed by tiny veinlets of more potassic feldspar grading to almost pure orthoclase (Or_{97.3}). Minute crystals of apatite are apparently confined to these potassium-rich veinlets. The most extreme sample (RP6) from Ruddon's Point contains, in addition to anorthoclase and zircon, a metamict

yttrio-niobate rich in heavy REE (HREE), U and Th, together with corundum.

FIDRA

A basanite intrusion at Fidra, close to the southern limits of the Midland Valley, contains a xenolith–megacryst suite that contrasts with those of the Ardross Fault vents. Abundant spinel ilmenite xenoliths are accompanied by wehrlite and clinopyroxenites (Hunter *et al.*, 1984). Megacrysts of alkali feldspar and magnetite are common, together with some composite anorthoclase–magnetite and anorthoclase–apatite megacrysts (Aspen *et al.*, 1990). Xenoliths of anorthoclase containing magnetite and chlorite pseudomorphs, probably after pyroxene, also occur. Rare xenoliths composed of approximately equal proportions of magnetite and apatite may represent localized facies within the anorthoclase protolith. Micas and amphiboles are absent and it is inferred that the xenoliths and megacrysts involving alkali feldspar, magnetite, apatite (and possible pseudomorphs after pyroxene) are fragments of coarse-grained syenite veins (with localized magnetite–apatite concentrations), crystallized from Na-, K-, Fe- and P-rich melts within wehrlite–clinopyroxenite host rocks. The Fidra alkali feldspars are notably more calcic than any other anorthoclases yet found in Scotland, consistent with their having had a higher temperature paragenesis.

SOUTHERN UPLANDS

South of the Southern Uplands fault, xenolith–megacryst occurrences are sparse although there are significant occurrences at three localities: Earnscluch, Hexpath and Burn-between-the-Laws.

Earnscluch

A sodic anorthosite xenolith (Lau24) comprises essentially unzoned oligoclase crystals, in a well-equilibrated fabric with triple grain boundaries meeting at angles of $\sim 120^\circ$. Sporadic development of melt patches appears to indicate a second original phase, probably a pyroxene. The sample is thus a rather pure, sodic anorthosite lacking magnetite, zircon or apatite.

Hexpath

A small (~ 10 mm), anorthoclase xenolith (Hex8), consists of roughly equidimensional feldspar crystals (0.5–2 mm diameter). Scanning electron microscope imaging shows it to be a two-feldspar rock containing Na-rich anorthoclase ($\text{An}_{16.8}\text{Ab}_{71.3}\text{Or}_{11.4}$) and a discrete, more potassic feldspar ($\text{An}_2\text{Ab}_{47.8}\text{Or}_{50.2}$). The xenolith encloses scarce, Fe-rich

orthopyroxene ($\text{En}_{51.2}\text{Wo}_{0.6}\text{Fs}_{48.2}$, Table 1) as well as discrete grains of ilmenite and Ti magnetite. Using the calibration of Ghiorso & Sack (1991), these oxides indicate equilibration at 639°C and at $\log f\text{O}_2$ of -19.98 (with respect to QFM) for an assumed pressure of 10 kbar. HEX8 (together with the Gribun xenolith, GRB117), is unique in providing an indicator of crystallization conditions (and also in containing orthopyroxene, indicating crystallization below the pigeonite inversion curve, despite its relatively Fe-rich character). An anorthoclase megacryst (HEX14a), 15 mm across, in the same basanite body, has a core of $\text{An}_{10.4}\text{Ab}_{69.3}\text{Or}_{20.3}$ and a rim of $\text{An}_{10.0}\text{Ab}_{62.5}\text{Or}_{27.5}$ with up to 0.28% BaO. It contains elongate apatite prisms and small blebs of chalcopyrite. Such large feldspars suggest the possibility of a pegmatitic anorthoclase source.

Burn-between-the-Laws

BBL24 is a xenolith measuring ~ 30 mm \times 12 mm, composed of $\sim 80\%$ anorthoclase and $\sim 20\%$ corundum enclosing small idiomorphic crystals of columbite. Other, highly corroded, anhedral columbite crystals lie within the earlier of two generations of cross-cutting calcite veinlets. Very small crystals of apatite occur within the feldspars. The assemblage anorthoclase–corundum plus a niobium-rich oxide mineral is similar to that of the peraluminous syenitic xenoliths from Loch Roag and Riddon's Point.

MINERAL CHEMISTRY

Principal attention was given to the alkali feldspars and, to a lesser extent, their associated parageneses. The trace-element chemistry of the major mineral phases (with the exception of magnetite) is given in Tables 2–5.

Micro-analytical techniques

Trace-element analyses of megacryst phases were made, using a Cameca ims-4f ion microprobe at Edinburgh University, using a combination of glass and secondary mineral standards. These included anorthoclase and sanidine, clinopyroxene, biotite, apatite, corundum and Nb oxide. Data for zircon and samarskite from Elie Ness and Loch Roag have been presented in an earlier paper (Hinton & Upton, 1991). For the major elements, comparison was also made with electron microprobe analyses of the same sample (but not at the same point of analysis). All measurements involved energy filtering to reduce the presence of molecular interferences. Measurements were made using an energy offset of either 75 eV (clinopyroxene, biotite and corundum) or 120 eV (apatite, feldspar and oxide phases). The presence of fluorides in

Table 2: Feldspar compositions: major and trace element determinations by ion microprobe analysis

Locality: Ruddon's Point	Burn-between-the-Laws				Holmbyre				Elie				Coalyard Hill				Fidra				Loch Roag				Gribun			
	BBL24		Core		Rim		Vein		HB87		HB88		Ness		EN-2B		CYD 13		FD86		RSM1		LR57		GRB117			
	Core	Rim	Core	Rim	Core	Rim	Vein	Br. Bl. CL	Core	Bulk*	Core	Bulk*	Core	Bulk*	Core	Bulk*	Core	Vein	Core	Vein	Core	Vein	Core	Vein	Core	Vein	Core	Rim
wt %	65.0	65.0	65.0	65.0	65.0	65.0	65.0	65.0	65.0	65.0	65.0	65.0	65.0	65.0	65.0	65.0	65.0	65.0	65.0	65.0	65.0	65.0	65.0	65.0	65.0	65.0	65.0	65.0
SiO ₂	20.0	20.3	19.3	19.3	19.3	19.3	19.3	19.3	19.3	19.3	19.3	19.3	19.3	19.3	19.3	19.3	19.3	19.3	19.3	19.3	19.3	19.3	19.3	19.3	19.3	19.3	19.3	19.3
Al ₂ O ₃	1.41	1.39	0.10	1.71	0.21	0.35	0.35	0.35	0.35	0.35	0.35	0.35	0.35	0.35	0.35	0.35	0.35	0.35	0.35	0.35	0.35	0.35	0.35	0.35	0.35	0.35	0.35	0.35
CaO	8.18	7.65	7.04	9.44	5.78	5.93	5.93	5.93	5.93	5.93	5.93	5.93	5.93	5.93	5.93	5.93	5.93	5.93	5.93	5.93	5.93	5.93	5.93	5.93	5.93	5.93	5.93	5.93
Na ₂ O	4.43	5.32	7.86	1.39	9.89	9.94	9.94	9.94	9.94	9.94	9.94	9.94	9.94	9.94	9.94	9.94	9.94	9.94	9.94	9.94	9.94	9.94	9.94	9.94	9.94	9.94	9.94	9.94
K ₂ O	99.1	99.7	99.3	99.3	100.7	101.9	101.9	101.9	101.9	101.9	101.9	101.9	101.9	101.9	101.9	101.9	101.9	101.9	101.9	101.9	101.9	101.9	101.9	101.9	101.9	101.9	101.9	101.9
Sum	1.1	1.1	2.9	2.1	2.1	6.6	6.6	6.6	6.6	6.6	6.6	6.6	6.6	6.6	6.6	6.6	6.6	6.6	6.6	6.6	6.6	6.6	6.6	6.6	6.6	6.6	6.6	6.6
B	57	48.8	322	51.7	65.5	1450	1450	1450	1450	1450	1450	1450	1450	1450	1450	1450	1450	1450	1450	1450	1450	1450	1450	1450	1450	1450	1450	1450
Ti	0.02	0.89	3.3	0.02	0.01	5.5	5.5	5.5	5.5	5.5	5.5	5.5	5.5	5.5	5.5	5.5	5.5	5.5	5.5	5.5	5.5	5.5	5.5	5.5	5.5	5.5	5.5	5.5
Zr	0.12	48.4	175	0.07	0.08	15.6	15.6	15.6	15.6	15.6	15.6	15.6	15.6	15.6	15.6	15.6	15.6	15.6	15.6	15.6	15.6	15.6	15.6	15.6	15.6	15.6	15.6	15.6
Nb	282	439	7740	608	380	2100	2100	2100	2100	2100	2100	2100	2100	2100	2100	2100	2100	2100	2100	2100	2100	2100	2100	2100	2100	2100	2100	2100
Fe	0.04	0.52	2.4	0.15	0.13	7.31	7.31	7.31	7.31	7.31	7.31	7.31	7.31	7.31	7.31	7.31	7.31	7.31	7.31	7.31	7.31	7.31	7.31	7.31	7.31	7.31	7.31	7.31
Li	13.7	13.2	43.0	4.4	148	130	130	130	130	130	130	130	130	130	130	130	130	130	130	130	130	130	130	130	130	130	130	130
Rb	0.05	0.1	0.11	0.03	0.70	0.68	0.68	0.68	0.68	0.68	0.68	0.68	0.68	0.68	0.68	0.68	0.68	0.68	0.68	0.68	0.68	0.68	0.68	0.68	0.68	0.68	0.68	0.68
Cs	4.8	0.52	2.3	7.1	2.5	1.9	1.9	1.9	1.9	1.9	1.9	1.9	1.9	1.9	1.9	1.9	1.9	1.9	1.9	1.9	1.9	1.9	1.9	1.9	1.9	1.9	1.9	1.9
Be	5.0	118	1150	21.3	8.0	163	163	163	163	163	163	163	163	163	163	163	163	163	163	163	163	163	163	163	163	163	163	163
Mg	98.8	255	5.0	47.5	31.1	312	312	312	312	312	312	312	312	312	312	312	312	312	312	312	312	312	312	312	312	312	312	312
Sr	211	581	26	14.6	29.0	326	326	326	326	326	326	326	326	326	326	326	326	326	326	326	326	326	326	326	326	326	326	326
Ba	—	—	—	—	—	—	—	—	—	—	—	—	—	—	—	—	—	—	—	—	—	—	—	—	—	—	—	—
Pb	83.0	85.2	69.0	85.1	25.3	29.3	29.3	29.3	29.3	29.3	29.3	29.3	29.3	29.3	29.3	29.3	29.3	29.3	29.3	29.3	29.3	29.3	29.3	29.3	29.3	29.3	29.3	29.3
La	130	130	108	101	18.1	30.5	30.5	30.5	30.5	30.5	30.5	30.5	30.5	30.5	30.5	30.5	30.5	30.5	30.5	30.5	30.5	30.5	30.5	30.5	30.5	30.5	30.5	30.5
Ce	—	—	—	—	—	—	—	—	—	—	—	—	—	—	—	—	—	—	—	—	—	—	—	—	—	—	—	—
Pr	—	—	—	—	—	—	—	—	—	—	—	—	—	—	—	—	—	—	—	—	—	—	—	—	—	—	—	—
Nd	—	—	—	—	—	—	—	—	—	—	—	—	—	—	—	—	—	—	—	—	—	—	—	—	—	—	—	—
Sm	—	—	—	—	—	—	—	—	—	—	—	—	—	—	—	—	—	—	—	—	—	—	—	—	—	—	—	—
Eu	2.31	5.91	0.05	0.54	0.47	1.07	1.07	1.07	1.07	1.07	1.07	1.07	1.07	1.07	1.07	1.07	1.07	1.07	1.07	1.07	1.07	1.07	1.07	1.07	1.07	1.07	1.07	1.07
Tb	—	—	—	—	—	—	—	—	—	—	—	—	—	—	—	—	—	—	—	—	—	—	—	—	—	—	—	—
Y	0.34	3.56	8.7	0.71	0.03	0.26	0.26	0.26	0.26	0.26	0.26	0.26	0.26	0.26	0.26	0.26	0.26	0.26	0.26	0.26	0.26	0.26	0.26	0.26	0.26	0.26	0.26	0.26
ppm	—	—	—	—	—	—	—	—	—	—	—	—	—	—	—	—	—	—	—	—	—	—	—	—	—	—	—	—
B	—	—	—	—	—	—	—	—	—	—	—	—	—	—	—	—	—	—	—	—	—	—	—	—	—	—	—	—
Ti	—	—	—	—	—	—	—	—	—	—	—	—	—	—	—	—	—	—	—	—	—	—	—	—	—	—	—	—
Zr	—	—	—	—	—	—	—	—	—	—	—	—	—	—	—	—	—	—	—	—	—	—	—	—	—	—	—	—
Nb	—	—	—	—	—	—	—	—	—	—	—	—	—	—	—	—	—	—	—	—	—	—	—	—	—	—	—	—
Fe	—	—	—	—	—	—	—	—	—	—	—	—	—	—	—	—	—	—	—	—	—	—	—	—	—	—	—	—
Li	—	—	—	—	—	—	—	—	—	—	—	—	—	—	—	—	—	—	—	—	—	—	—	—	—	—	—	—
Rb	—	—	—	—	—	—	—	—	—	—	—	—	—	—	—	—	—	—	—	—	—	—	—	—	—	—	—	—
Cs	—	—	—	—	—	—	—	—	—	—	—	—	—	—	—	—	—	—	—	—	—	—	—	—	—	—	—	—
Be	—	—	—	—	—	—	—	—	—	—	—	—	—	—	—	—	—	—	—	—	—	—	—	—	—	—	—	—
Mg	—	—	—	—	—	—	—	—	—	—	—	—	—	—	—	—	—	—	—	—	—	—	—	—	—	—	—	—
Sr	—	—	—	—	—	—	—	—	—	—	—	—	—	—	—	—	—	—	—	—	—	—	—	—	—	—	—	—
Ba	—	—	—	—	—	—	—	—	—	—	—	—	—	—	—	—	—	—	—	—	—	—	—	—	—	—	—	—
Pb	—	—	—	—	—	—	—	—	—	—	—	—	—	—	—	—	—	—	—	—	—	—	—	—	—	—	—	—
La	—	—	—	—	—	—	—	—	—	—	—	—	—	—	—	—	—	—	—	—	—	—	—	—	—	—	—	—
Ce	—	—	—	—	—	—	—	—	—	—	—	—	—	—	—	—	—	—	—	—	—	—	—	—	—	—	—	—
Pr	—	—	—	—	—	—	—	—	—	—	—	—	—	—	—	—	—	—	—	—	—	—	—	—	—	—	—	—
Nd	—	—	—	—	—	—	—	—	—	—	—	—	—	—	—	—	—	—	—	—	—	—	—	—	—	—	—	—
Sm	—	—	—	—	—	—	—	—	—	—	—	—	—	—	—	—	—	—	—	—	—	—	—	—	—	—	—	—
Eu	—	—	—	—	—	—	—	—	—	—	—	—	—	—	—	—	—	—	—	—	—	—	—	—	—	—	—	—
Tb	—	—	—	—	—	—	—	—	—	—	—	—	—	—	—	—	—	—	—	—	—	—	—	—	—	—	—	—
Y	—	—	—	—	—	—	—	—	—	—	—	—	—	—	—	—	—	—	—	—	—	—	—	—	—	—	—	—

SiO₂ assumed to be 65% (except XRF bulk analysis of HB88 and CYD13). Cathodoluminescence colours: Bl., blue; Br.Bl., bright blue; Gr., green. b.d., below detection limit; —, not analysed. *XRF.

Table 3: Trace element compositions of corundum by ion microprobe analysis

Locality:	Ruddon's Point			Burn-between-the-Laws			Loch Roag		Loch Roag	
Sample:	RP6			BBL24			RSM2		LR1	
<i>Element</i>										
B	0.073	0.089	0.064	—	0.03	0.15		<0.002	—	—
Ga	402	—	—	—	555	—	—	238	—	—
Si	18.1	306	13.5	—	18.5	21.1	4.0	315	25.2	14.9
Ti	17.2	340	1120	154	950	2570	43.2	390	110	531
Zr	0.014	0.047	0.28	—	0.04	0.74	0.035	0.045	0.06	0.06
V	2.6	93	2.7	25.8	45.9	—	6.2	12	13.0	19.9
Nb	0.007	0.28	5.02	—	1.31	59.0	0.37	1.3	<0.06	8.2
Cr	0.83	—	0.02	—	0.05	—	0.34	0.29	0.08	0.04
Mn	1.38	0.45	51.1	—	0.98	6.69	0.46	0.60	0.65	4.39
Fe	5850	7120	9220	2530	5140	3910	4750	7240	7800	12060
Co	0.22	0.24	—	—	0.33	—	0.22	0.28	0.35	0.48
Li	0.002	<0.002	0.027	—	0.015	0.006	—	<0.002	—	—
Na	2.1	4.6	—	1.9	2.7	16.1	1.3	1.49	3.88	3.46
K	3.9	5.6	3.7	—	3.6	14.7	0.5	1.25	7.25	5.44
Rb	0.075	0.040	0.057	—	0.005	—	—	—	—	—
Cs	0.065	0.040	0.064	—	0.03	—	—	—	—	—
Be	0.06	0.21	0.31	0.12	0.27	2.6	—	—	—	2.31
Mg	4.8	1.7	4.8	—	13.0	13.3	7.3	15.3	1.03	3.07
Ca	8.3	1.8	159	6.1	4.4	10.0	1.8	2.2	2.55	1.25
Sr	0.045	0.038	0.068	—	0.02	—	0.016	0.041	<0.02	<0.02
Ba	0.068	0.052	0.006	—	0.02	0.12	—	0.52	<0.09	<0.09
Pb	4.3	0.57	4.6	—	<0.01	—	—	—	—	—
La	0.005	0.005	0.053	—	0.01	0.98	—	—	<0.03	0.04
Ce	<0.002	0.022	0.207	—	<0.002	1.28	—	0.041	<0.06	0.14
Y	0.004	0.003	0.034	—	<0.002	0.04	—	0.015	<0.03	<0.03
Th	0.01	<0.01	0.32	—	0.01	—	—	0.1	—	—
U	<0.01	0.09	0.04	—	0.01	—	—	0.1	<0.2	1.3

—, not analysed. Eu analysed but below detection limit all cases (<0.005). Al₂O₃ assumed to be 99%.

apatite was assessed using the CaF and CeF peaks. Tb could not be measured in all apatites because of the presence of CeF. Corrections were made for the overlap of the LREE oxides on the HREE and BaO on Eu. Concentrations were calculated using ion yields measured relative to Si (for silicates), Al and Al²⁺ (for corundum) and Nb (for oxides). Because ion probe analyses were not obtained at the same point as the electron probe analyses (not given here) the SiO₂ of the feldspar megacrysts was assumed to be 65 wt %. The major element totals based on secondary standards averaged just under 100%. In general there is good agreement (usually better than 10%) between major element data obtained by

electron microprobe and ion microprobe measurements (see Table 3).

Feldspar

Reconnaissance electron and ion microprobe data for anorthoclase megacrysts from Elie Ness and a neighbouring vent at Brownhills were presented by Mason *et al.* (1982). In the feldspars investigated in the present study, veins and/or patches appear to have been secondarily altered. The unaltered (primary) feldspars analysed by ion microprobe for trace elements (Table 2) are

Table 4: Major and trace element compositions of clinopyroxene, biotite and apatite; determinations by ion microprobe, apart from those major elements (asterisked analyses) determined by electron microprobe

Locality:	Loch Roag			Fidra		Gribun			
Sample no.:	LRS7			FD 305	FD 86	GRB 117		MLL6	
Mineral:	Cpx*	Biot*	Apat*	Apat	Apat	Cpx*	Apat	Cpx*	Apat
<i>wt %</i>									
SiO ₂	46.0	33.8	0.22	—	0.40	50.7	—	47.6	0.31
Al ₂ O ₃	8.66	15.4	—	—	0.004	3.3	—	6.25	0.001
FeO	11.4	19.6	0.49	—	0.29	11.7	0.27	9.15	0.13
MgO	9.01	10.2	0.32	—	0.07	10.7	0.14	10.76	0.11
CaO	20.6	0.008	52.1	56.0	56.0	20.2	56.0	21.44	56.0
Na ₂ O	1.80	0.39	—	—	0.39	2.14	0.41	1.49	0.31
K ₂ O	—	9.1	—	—	0.005	—	—	—	0.001
TiO ₂	1.54	6.9	—	—	—	0.54	0.17	1.77	—
MnO	0.26	0.18	0.12	—	0.22	0.51	0.17	0.23	0.06
P ₂ O ₅	—	—	38.4	41.8	—	—	—	—	—
F	—	0.20	1.6	3.5	—	—	—	—	—
Cl	—	—	0.40	0.21	—	—	—	—	—
<i>ppm</i>									
B	0.38	0.78	—	—	0.34	0.61	0.34	0.19	0.23
Zr	567	101	22.3	—	—	213	6.92	203	—
Hf	18.7	—	—	—	—	—	—	—	—
Nb	4.00	117	—	—	—	1.64	—	1.4	—
Ta	0.63	—	—	—	—	—	—	—	—
Li	1.60	4.76	—	—	0.64	9.99	0.64	2.71	0.23
K	51.3	—	—	—	44.6	10.1	36.5	1.64	10.6
Rb	—	1.1	—	—	<0.01	—	—	—	—
Be	1.43	0.24	—	—	<0.01	3.12	<0.01	1.86	<0.01
Sr	608	470	8769	2518	1655	112	2610	338	4040
Ba	0.57	7473	65.8	57.8	15.9	3.02	316	0.77	16.3
La	31.6	—	907	579	3595	26.8	3567	10.5	365
Ce	109	0.030	1905	1215	6628	91.5	6858	37.7	864
Pr	17.9	0.038	235	150	688	14.5	730	6.91	110
Nd	87.3	0.15	1031	695	2649	73.6	3020	3.65	520
Sm	18.0	0.32	140	103	410	16.2	513	9.29	102
Eu	5.17	—	48.2	36.1	94	5.29	122	2.7	32.6
Gd	14.1	—	85.3	70.9	297	15.9	390	8.19	81.4
Tb	1.89	—	9.66	8.90	—	2.33	42.9	1.03	7.85
Dy	10.6	—	47.8	46.2	173	14.3	201	5.26	38.8
Ho	1.67	—	7.29	7.43	26.9	2.30	32.5	0.93	5.03
Y	32.1	0.24	145	199	677	47.6	629	18.8	138
Er	4.10	—	15.8	14.6	69.1	6.41	70	2.01	12.3
Tm	—	—	1.78	1.74	8.6	1.02	10.9	0.28	1.25
Yb	3.51	—	8.99	6.91	40.7	6.27	43.3	1.64	5.06
Lu	—	—	1.04	0.55	5.31	1.08	5.65	0.18	0.64
Th	—	—	11.2	3.98	48.6	0.83	124	—	3.88
U	—	—	1.73	1.07	13	0.010	30.25	—	1.07

Table 5: Major and trace element compositions of Nb-rich oxides: determinations by electron microprobe (EP) and ion microprobe (IP) analysis

Locality:	Burn-between-the-Laws		Ruddon's Point			Loch Roag			
Sample no.:	BBL24		RP6			RSM1/2			
Mineral:	Columbite		Yttrio-niobate			Samarskite			
Technique:	EP	IP	EP	EP	IP	EP	IP	IP	IP
<i>wt %</i>									
TiO ₂	3.26	3.53	1.42	0.97	0.72	16.8	16.3	24.4	14.8
FeO	13.4	[13.4]	0.12	4.39	3.43	1.87	1.51	1.75	1.27
MnO	6.00	[6.0]	0.15	0.26	0.24	0.060	0.032	0.041	0.025
CaO	—	0.058	1.27	3.52	1.72	4.12	2.65	4.74	2.90
ZrO ₂	1.33	2.58	0.30	1.17	1.67	0.27	0.16	0.22	0.21
Nb ₂ O ₅	72.0	[72.0]	42.0	45.0	[45.0]	34.1	[34.1]	[34.1]	[34.1]
Ta ₂ O ₅	3.49	4.87	0.37	2.69	2.43	2.22	1.93	1.12	1.57
Y ₂ O ₃	—	0.62	10.5	4.93	4.47	1.87	1.88	2.15	1.46
ThO ₂	—	0.073	16.2	24.1	19.2	19.8	14.8	5.99	9.47
UO ₂	—	0.014	1.86	3.26	4.55	0.39	0.27	0.075	0.041
Sum	99.47		98.49	95.94		99.47			
<i>ppm</i>									
Al	—	102	—	—	831	—	433	686	376
Si	—	13.4	645	4426	1019	514	1.1	14.6	2.87
Sc	—	879	—	—	638	—	—	115	99.3
V	—	35.1	—	—	25.3	—	115	212	111
Cr	—	0.6	—	—	0.3	—	0.77	2.4	1.03
Na	—	30.8	—	—	1320	—	402	629	308
Mg	—	1892	—	—	188	—	100	124	19.6
Sr	—	0.8	—	—	417	—	—	—	—
Ba	—	—	—	—	106	—	—	3	9
La	—	5.46	9720	890	506	22400	17500	21400	20550
Ce	—	70.2	57900	7050	6701	85000	75600	84500	70260
Pr	—	—	11000	1700	1755	9910	9489	10860	8401
Nd	—	108	52900	10200	10150	30500	31270	35250	26430
Sm	—	60.3	18100	4720	3989	—	5297	5819	4451
Eu	—	2.99	—	—	181	—	506	683.2	601
Gd	—	169	23500	6720	3825	4860	3718	6428	2918
Tb	—	53.9	—	—	913	—	770	906	606
Dy	—	632	21500	8000	6263	—	5079	5985	3481
Ho	—	185	—	—	1364	—	856	782	593
Er	—	852	7610	4160	4504	1310	2318	2052	1370
Tm	—	187	—	—	790	—	303	269	160
Yb	—	1585	5460	4960	5646	—	1532	865	771
Lu	—	257	—	—	787	—	179	76.3	63

—, not analysed; [], concentrations assumed for IP calculations.

all anorthoclases, with the exception of sanidine from Loch Roag. The unaltered areas generally have very constant major and trace element chemistry and only in one sample (Loch Roag, RSM1) was strong zoning

observed (sanidine to anorthoclase). Feldspar in GRB117 exhibits some zoning (core to rim) from 15 to 7% An.

There are differences of up to three orders of magnitude between the LREE (specifically, La and Ce) contents of

the analysed feldspars (Fig. 4). The feldspars can be subdivided on the basis of their REE, Ba and Sr contents into: (1) a group with high LREE (>20 ppm La) and low Ba and Sr contents (RP6, BBL24 and RSM1); (2) a group with very low La and Ce contents (<1 ppm) and moderate Ba and Sr contents (HB87, CYD10 and CYD13); (3) those with intermediate levels of LREE (1–12 ppm La) and moderate to high contents (>1500 ppm) of Sr and Ba (namely, EN2B, FD86, GRB117 and LR57). It is clear that the xenoliths (RSM1, RP6 and BBL24) containing corundum and Nb oxides are also those that contain the most REE-rich feldspars, although these are distinctly poor in Ba and Sr. The Coalyard Hill (CYD10 and CYD13) and Holmbyre (HB87) feldspars differ from those of the corundum-bearing assemblages in having very low REE contents as well as being very poor in CaO (Fig. 4). Although the analysed feldspars are monomineralic megacrysts, other feldspars from the same vents (with similar major element chemistry) are accompanied by biotite, apatite and calcite (the last possibly secondary after pyroxene).

Some outer rims of individual crystals exhibit various degrees of secondary alteration, typically along veins; in general, such alteration can be readily distinguished by an increase in the potassium content of the feldspar from 1–4% K₂O to 7–9% K₂O. Two samples also show replacement of anorthoclase by very pure K-feldspar. The major and trace element compositions of these secondary feldspars are given in Table 2. It is clear, however, that the type of alteration varies between megacrysts and, also, that more than one type of alteration may be present within a single crystal. Cathodoluminescence (CL) studies of BBL24 revealed three different types of feldspar (Fig. 3c and d): the (primary) cores of the feldspar crystals show green luminescence whereas diffuse secondary alteration along cleavage planes and irregular fractures gave rise to feldspar that luminesces (dull) dark blue. The xenolith is traversed (as is commonplace for other xenoliths and megacrysts) by fine-scale veinlets of fairly pure calcite (bright orange CL) containing small quantities of Mn and Fe. Two generations of veinlets are identifiable: earlier, slightly broader veinlets are symmetrically rimmed by feldspar exhibiting bright (pale) blue CL. This 'bright blue feldspar' has been generated adjacent to the calcite veinlets from both the dull blue and green luminescing feldspar. All are then traversed by fine-scale late-stage veinlets that are not associated with any alteration of their feldspar side-walls. Both varieties of blue-CL feldspar have notably higher K/Na values than the feldspar luminescing green. The change from green to blue cathodoluminescence is well defined in both major and trace element chemistry. There is a notable increase in K, with concomitant rise in Rb and Cs. An increase in Ba can also be explained, in part, by the increased ease of partitioning of Ba into

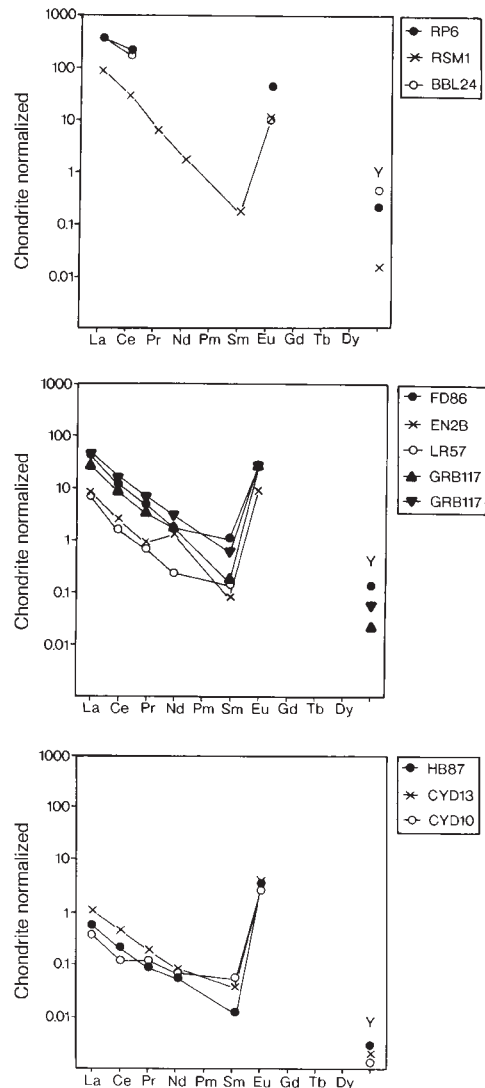


Fig. 4. Chondrite-normalized REE patterns for anorthoclases and sanidines from Scottish megacryst–xenolith assemblages. The three diagrams are arranged in order of decreasing REE content, the most enriched being from corundum-bearing samples at Riddon's Point (RP6), Loch Roag (RSM1) and Burn-between-the-Laws (BBL24). Ion microprobe data. It was not technically possible on the ion microprobe to determine REE heavier than Eu. Yttrium values are included for reference. Chondrite values used in normalization are from Anders & Grevesse (1989).

feldspar as the Or content increases. It should be noted, however, that the (green) host feldspar is unusually poor in Ba. In contrast, CaO decreases from the green to the blue luminescing feldspar, as do Sr, Fe and LREE. The 'bright blue' vein feldspar is not readily distinguishable from the dull blue luminescing feldspar in terms of major elements. However, whereas elements which strongly follow K (e.g. Rb and Cs) are unchanged, there is marked

increase in Li, B, Mg, Ca, Ti, Sr, Nb and Fe. For some elements there is, therefore, a reversal of the trend observed between green and dull blue luminescing feldspars. Although it is not known whether the increase in trace elements is due to sub-microscopic inclusions, it is clear that the strong change in luminescence is accompanied by a large increase in Fe and Ti.

The origins of feldspar CL have been the subject of much disagreement in the literature. Blue CL has been variously attributed to activations involving Ti (Mariano, 1988), Ga (De St Jorre & Smith, 1988), REEs (Laud *et al.*, 1971) and also to structural defects (Walker, 1985). Unpublished data (D. Stirling & A. Finch, personal communication, 1997) indicate a relationship between the intensity of blue CL in some feldspars and Al content. This may result not from activation, but rather substitution of Al into feldspar, which may promote structural defects, which cause luminescence. Other substitutions may similarly give rise to such defects and hence to blue CL. In the present example, we note that the areas of brightest blue CL are those of feldspar with the greater concentration of dopant ions. Green CL in feldspar is generally considered to arise from a combination of the blue and a yellow excitation. Yellow CL is believed to result from Mn^{2+} activation (Walker, 1985) although we observed no relationship between the Mn content of these feldspars and the intensity of the inferred yellow excitation.

The variations in the BBL24 feldspars contrast to those observed in RP6 (Table 2), where alteration initially involved an increase in Fe and alkaline earths, without changing the bulk chemistry or REE contents. More pervasive alteration led to a marked drop in the alkaline earths, including Ba, with a very large increase in Fe. Whereas La and Ce decrease only slightly, Eu falls substantially. This is consistent with the supposition that Eu exists principally as Eu^{2+} within the feldspar lattice, showing strong behavioural similarity to Sr^{2+} .

The trace element chemistry of the Coalyard Hill megacrysts is markedly different from that of the other feldspars studied. Recrystallization along veins has produced pure end-member sanidine with very low concentrations of alkaline earth elements and LREE as well as Fe and Ti. In the K-feldspar vein in CYD13, even Ba is remarkably low in comparison with the primary host feldspar, despite the preference of this element for the Or end-member.

It is clear that the original feldspars were subject to changes after their crystallization and it is inferred that the high K feldspars formed at relatively low temperatures along cracks and grain boundaries. As the alteration is always accompanied by a marked K increase, yet the bulk feldspars are not particularly K rich, there is no reason to suspect that all of the feldspar has been altered or that the extremes in REE content observed between

megacrysts are secondary in nature. In brief, we conclude that these compositional modifications occurred in the protoliths before incorporation as xenocrysts in the host basalts.

Corundum

The Loch Roag corundums show asterism as well as fine-scale concentric oscillatory zonation (see Irving, 1986). In thin section, they are colourless except for brown (euhedral) core regions and brownish coloration caused by oriented micro-inclusions of rutile (Fron del, 1954) along radiating zones whose axes are 60° apart (Fig. 5). We infer that these inclusions lie in the basal plane, perpendicular to the second-order prism faces (1120), bisecting the colour zoning at right angles (see Tait, 1959). As Ti_2O_3 and Fe_2O_3 (haematite) are both isostructural with corundum, significant solid solution may be expected. However, ilmenite–corundum systems often demonstrate broad solvi (see Sheikh & Irvine, 1993) as a result of entropy changes associated with ordering of the ilmenite. According to Fron del (1954), Ti^{3+} , substituting for Al^{3+} , exsolves from corundum as rutile during slow annealing in an oxidizing environment. In thin section the brownish coloration in the crystals may be due to the presence of both rutile needles and haematite plates exsolved from the corundum. Electron microprobe analysis from core to rim of one crystal (LR1), ~ 30 mm diameter, reveals a minor variation in Fe/Al ratio which correlates with the large number of fine-scale oscillatory zones. The total Fe content (expressed as 'FeO'), ranges from a minimum of 0.91% at the edge to a maximum of 2.08% at the core. Ti (as TiO_2) and MnO contents are generally at, or below, the electron microprobe detection limits but have their highest values (0.093% and 0.019%, respectively) in the Fe-rich core. These variations are supported by the ion probe measurements (Table 3). Corundum can dissolve up to 20% Fe_2O_3 in air at 1 atm PO_2 at $1400^\circ C$, falling to $\sim 10\%$ at $1100^\circ C$ (Muan & Gee, 1955) and it is concluded that the Fe-rich core crystallized at higher temperatures than the remainder of the crystal. No minor element differences could be detected between the colourless and the brownish radiating zones in the LR1 corundum.

The blue colour in corundum (as viewed megascopically) has been variously linked to trace amounts of Fe^{2+} , Fe^{3+} , Ti^{3+} and Ti^{4+} . Ferguson & Fielding (1971) attributed the colour to $Fe^{2+}-O-Ti^{4+}$ charge transfer but these conclusions were not supported by Matson & Rossman (1988), who favoured $Fe^{2+}-O-Fe^{3+}$ superexchange. Our observations that the intensity of the blue colour appears independent of Ti content support a charge transfer mechanism involving Fe alone. The fine-scale oscillatory zoning in the Loch Roag corundums

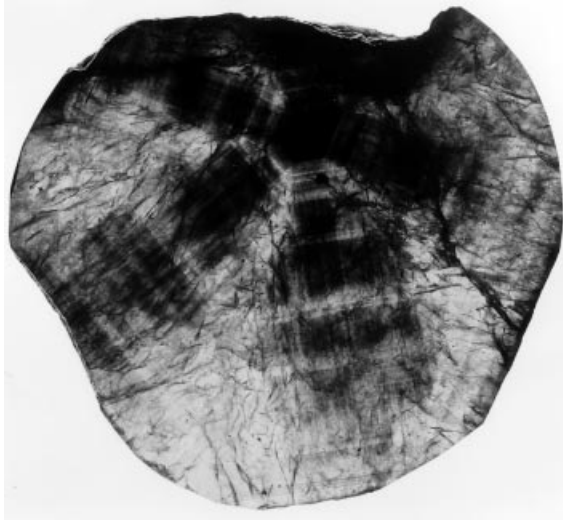


Fig. 5. Photomicrograph of corundum (LR1) from Loch Roag. The crystal has ~25 mm diameter and shows concentric oscillatory zonation, radiating (brownish) coloured zones and a dark Fe-rich core.

points to crystallization from a melt in which P , T and/or composition were fluctuating during megacryst growth.

Ion microprobe analyses were made of corundums from three localities (samples BBL24, Burn-between-the-Laws; RP6, Rudden's Point; RSM2, Loch Roag). Representative trace element analyses are presented in Table 3: analyses are selected to indicate the full range in chemical zoning and are given in order of increasing Ti content for each sample. In all four analysed corundums, the principal substituting elements are Fe and Ti. Although up to 300 ppm Si was observed, it is not clear how much may be ascribed to surface contamination. Na and K values may also be too high as a result of surface contamination and probably do not exceed 2 and 4 ppm, respectively.

Cathodoluminescence studies of the BBL24 corundum demonstrate the presence of zonation (not otherwise discernible), with luminescence changing from deep to lighter brown from the cores to the rims (Fig. 3b). Oscillatory zoning is manifest in terms of alternating light and dark CL bands. An ion microprobe traverse was made across one such zone (Fig. 6). Analyses were made by moving the sample beneath the primary beam, in 10 μm steps. At each step a single measurement was made of the secondary ion counts at masses 9 (Be), 13.5 (Al^{2+}), 48 (Ti), 56 (Fe) and 93 (Nb). Count rates, normalized to Al^{2+} , were converted to concentrations by reference to point analyses made in the core of the crystal. The broad change from darker to lighter brown CL colouring correlates with the decrease in Fe from centre outwards. Whereas the Fe content is highest in the core, the rim also shows notable Fe and Ti enrichment. Although Be (<3 ppm) follows Ti closely, Nb variations are even more

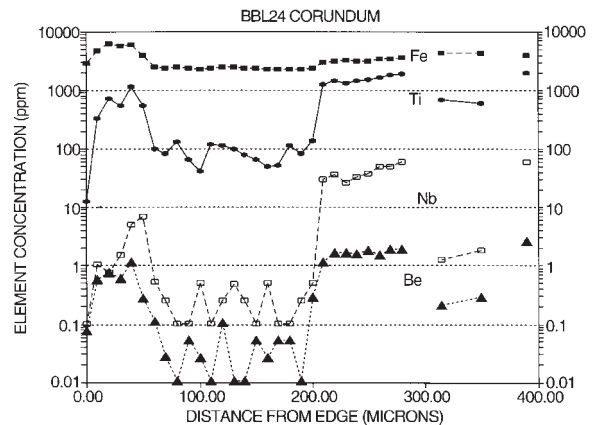


Fig. 6. Ion microprobe traverse of corundum crystal from Burn-between-the-Laws sample BBL24 showing variation in Fe, Ti, Nb and Be.

extreme (although still tending to correlate with Ti) and there is notable Nb deficiency in the outer rim. We conclude that the incorporation of individual elements changed during growth, either because of concentration changes in the melt from which the corundum was growing, or because of changes of the physical conditions attending growth. Whereas Fe^{3+} can fit within the corundum structure, the Ti^{4+} does not appear to be balanced by any coupled substitution. The poor fit of Ti within the corundum lattice at lower temperatures and pressures can also be inferred from the exsolution of fine needles of rutile in some crystals.

The spatial resolution of the ion probe beam was insufficient to resolve the fine-scale oscillatory zoning observed in CL. A second, higher spatial resolution, traverse was made along the same line by moving the sample in 2 μm (rather than 10 μm) steps beneath the primary beam and using a field aperture to select only ions from the central few microns of the sputtered area. Although the losses in secondary ion transmission with increase in spatial resolution were such that only Ti and Fe intensities could be measured, a clear correlation was observed between the CL oscillatory zones and Ti (and hence also Nb and Be) concentrations. The brightest CL correlated with the lowest Ti zones. It is accordingly inferred that the CL is quenched by the presence of Fe and Ti and that the intrinsic luminescence is due to other factors.

In contrast to the feldspar crystals, however, which are generally uniform in major and trace element composition (when not subject to later alteration), the corundums provide evidence for rapidly changing physico-chemical conditions during growth. The presence of disrupted growth zoning and the rounded morphology of many of the crystals suggest that the corundums formed

early and were partially resorbed before the crystallization of the feldspar.

CL of corundum may be due to several causes and the brown luminescence, rather than a single colour from the visible spectrum, hints at two or more distinct emissions. Activation of corundum CL by transition metal ions such as Ti^{3+} is known (Reisfeld *et al.*, 1987), but a variety of defect centres in corundum are recognized (e.g. Kotomin *et al.*, 1994) and these may also relate to luminescence. Ti^{3+} -doped alumina has been identified for laser applications and is characterized by emissions at 410 and 740 nm. Ion probe analysis demonstrates that the alternating light and dark brown CL zones correlate with changes in Ti content, suggesting some form of Ti-related activation mechanism. Emission in the violet or blue part of the visible spectrum is clearly not present, and a complex activation mechanism, possibly involving multivalent Ti and/or charge transfer to Fe, may be responsible for the observed CL.

Apatite

The feldspar megacrysts occasionally contain inclusions of magnetite and apatite (e.g. FD86). Furthermore, some xenoliths show anorthoclase in an equilibrated textural relationship with apatite, magnetite and clinopyroxene (e.g. samples LR57 and GRB117). These observations prompted the analysis of apatite and magnetite in samples FD305 (apatite–magnetite xenolith, Fidra) and MLL6 (apatite–magnetite–salite xenolith, Gribun). Data are presented in Table 4.

The compositions of two of the apatites (FD86 and GRB117) are virtually identical and the associated feldspars are also remarkably similar (Table 2). It may consequently be inferred that, although FD86 is a virtually monomineralic anorthoclase megacryst, it was derived from a feldspar–pyroxene–apatite–magnetite rock similar to the FD86 xenolith. The apatites of samples LR57, MLL6 and FD305 have similar REE contents (Table 4; Fig. 7) and are, accordingly, likely to have come from similar sources. This conclusion is supported by the compositional similarity of the pyroxenes in MLL6 and FD305. The two Gribun apatites show wide variation in absolute abundances, with GRB117 having a *ca.* $\times 14$ enrichment in LREE relative to MLL6. A less extreme, but still wide variation in values is shown by the Fidra apatites (FD86 and FD305). Values for the Loch Roag apatite are commensurate with those given by Menzies & Halliday (1988). The majority of the samples analysed have REE contents notably higher than the apatite megacrysts reported by Irving & Frey (1984).

Clinopyroxene

Compositions of the most highly evolved B-Group pyroxenes from Scotland are presented in Table 1. Whereas

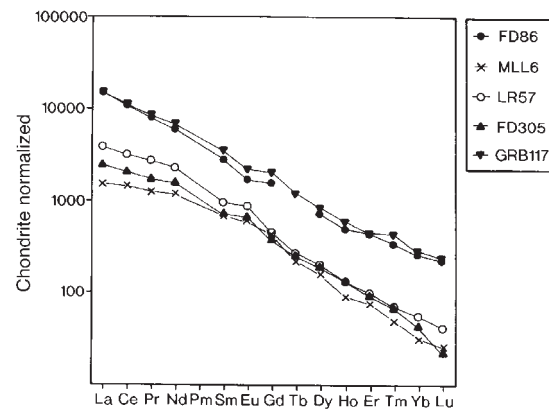


Fig. 7. Chondrite-normalized REE patterns for apatites from Fidra (FD), Gribun (MLL and GRB) and Loch Roag (LR). Chondrite values for normalization from Anders & Grevesse (1989).

there are no precise geobarometric indicators, the relatively jadeitic compositions of some (Al_2O_3 up to 10%, $Na_2O > 2\%$) point to a high-pressure paragenesis in the 5–15 kbar range (Thompson, 1974). As noted above, the pyroxenes in LR57 and MLL6 have similar major element compositions, with relatively high Al_2O_3 contents (6–9 wt %). Although the absolute REE contents differ by a factor of ~ 2 , the overall normalized patterns are comparable (Fig. 8). In contrast, whereas the absolute LREE concentrations in the GRB117 pyroxene resemble those of LR57, the former shows a more sinusoidal pattern. Rather less complete REE data for a pyroxene megacryst from Loch Roag were given by Menzies & Halliday (1988). The REE abundances for the analysed Loch Roag and Gribun clinopyroxenes are notably higher than those of other pyroxene megacrysts quoted by Irving & Frey (1984).

Nb- and Nb–REE-rich oxides

The Nb-rich oxides (columbite, ilmenorutile, yttrio-niobate and samarskite) occur exclusively in the peraluminous assemblages. Electron microprobe analyses of ilmenorutile, yttrio-niobate and samarskite were given by Aspen *et al.* (1990). Samarskite has $\sim 34\%$ Nb_2O_5 , 20% ThO_2 and 22% REE_2O_3 . Further data for samarskite were presented by Hinton & Upton (1991) and new analyses are given in Table 5, together with analyses of columbite. Nb–REE-rich oxides, analogous to yttrio-niobate and samarskite, are known from inclusions in basalt-hosted corundums around the world (Guo *et al.*, 1996b). Whereas the three analysed samples (Table 5) have varying proportions of Nb, REE and Th, the chondrite-normalized REE patterns (Fig. 9) are distinctive in having $La \ll Ce$ and marked negative Eu anomalies.

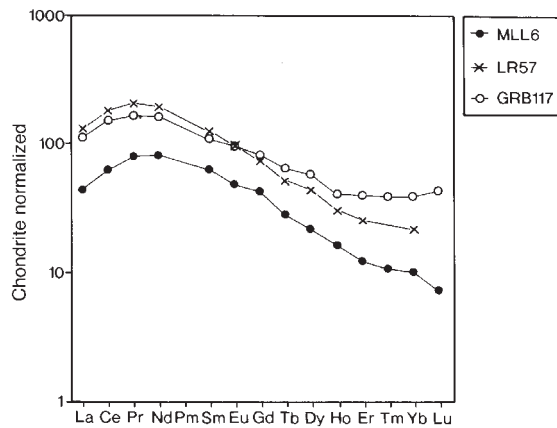


Fig. 8. Chondrite-normalized REE patterns for Group B megacryst-xenolith pyroxenes from Gribun (MLL and GRB) and Loch Roag (LR). Chondrite values for normalization from Anders & Grevesse (1989).

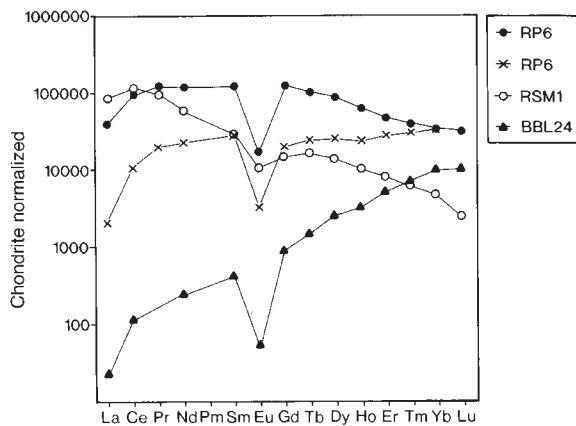


Fig. 9. Chondrite-normalized REE patterns for yttrium-niobate (RP6), samarskite (RSM1) and columbite (BBL24). Chondrite values for normalization from Anders & Grevesse (1989).

Guo *et al.* (1996*b*) noted that of all the inclusions recorded from basalt-hosted corundums, Nb-Ta oxides are the most abundant and persistent. They pointed out that the columbites have a distinctive composition, with high TiO_2 (up to 17 wt %) and low Ta_2O_5 (typically <4%) comparable with columbites from carbonatites. However, the columbites in this study (BBL24) have TiO_2 ~3.4% with Ta_2O_5 from 3.5 to 4.9%.

OXYGEN ISOTOPE RATIOS

Oxygen isotope ratios were measured for mineral separates of selected megacrysts (feldspars, zircons, biotites and corundums; Table 6) at the University of Wisconsin, using laser heating, BrF_3 reagent and gas-source mass

spectrometry (Valley *et al.*, 1995). Sample sizes ranged from 0.4 to 3.9 mg with most samples between 1 and 2 mg. All minerals except feldspar were analysed as single crystals or as small pieces of crystals and were pre-fluorinated overnight to remove hydrous contaminants. Feldspars were analysed as powder using a special air-lock sample chamber that permits samples to be out-gassed at vacuum overnight without fluorination and then placed into the fluorination chamber one at a time for analysis (Spicuzza *et al.*, 1998). This procedure prevents premature reaction of feldspar powder during pre-fluorination. Analyses were normalized to a value of $\delta^{18}\text{O} = 5.80$ for UWG-2, a garnet standard (Valley *et al.*, 1998) that was analysed from four to seven times each day. This normalization entailed small daily corrections of from +0.11 to -0.12‰. The average precision of standard analyses is ± 0.09 ‰ (1 SD) with average uncertainty in the mean of 0.04‰. Values of $\delta^{18}\text{O}$ are reported in the standard per mil notation relative to VSMOW.

The measured values of $\delta^{18}\text{O}$ are consistent with equilibrium fractionations from a single reservoir at 800°C for all of the minerals except feldspar. Values for feldspar are consistently high, from 6.60 to 13.76‰, 1–8‰ above the equilibrium value. Selective alteration and isotope exchange in feldspar is commonly observed because of its open crystal structure, which causes intracrystalline oxygen diffusion to be fast relative to other minerals, and because of its steady dissolution and alteration to secondary minerals (Eiler *et al.*, 1993). Many of the feldspars in this study have micro-fractures with calcite veining. Such fracturing would greatly facilitate secondary oxygen exchange with circulating fluids and at low temperatures this would raise the $\delta^{18}\text{O}$ of the feldspar without necessarily affecting other minerals.

The most significant aspect of the oxygen isotope ratios reported here is the homogeneity among samples from widely scattered localities. At Elie Ness, seven analyses of zircon range from 4.49 to 5.03 (average $\delta^{18}\text{O} = 4.78 \pm 16$ ‰). Four of these analyses are of single crystals, indicating that this tight clustering of values is not the result of averaging. These zircon compositions are similar to, but slightly lower than, values of mantle-derived zircon megacrysts from kimberlite in South Africa and Siberia ($\delta^{18}\text{O} = 4.7$ – 5.9 ‰, Valley *et al.*, 1998) and overlap with compositions of zircons from Tertiary granites in western Scotland (Gilliam & Valley, 1997; Monani & Valley, 1998). Samples of biotite, clinopyroxene and corundum from three other localities (Table 6) range from 4.65 to 5.39‰, consistent with equilibration with zircon ($\delta^{18}\text{O} = 4.8$) at 800°C. This consistency of values suggests derivation of the megacrysts from an igneous reservoir, homogeneous with respect to $\delta^{18}\text{O}$ in the sub-continental mantle of Scotland, and it rules out an origin for these minerals in crustal lithologies such as meta-sediment or evolved high $\delta^{18}\text{O}$ igneous rocks.

Table 6: Oxygen isotope ratios of mineral separates from Scottish mantle megacrysts

Sample	Mineral	$\delta^{18}\text{O}\text{‰}$	$\delta^{18}\text{O}\text{‰}$
		raw	VSMOW
Ardmucknish			
ARD-1	feldspar ^p	7.48, 7.87	7.78
ARD-7	feldspar ^p	13.55, 13.76	13.76
Briggs o' Fidra			
BOF-1	feldspar ^p	6.48, 6.50	6.60
BOF-30	feldspar ^p	7.10	7.21
Burn-between-the-Laws			
BBL-33	biotite	5.48	5.36
Coalyard Hill			
CYD-H13	feldspar ^p	7.32, 7.25	7.39
CYD-H16	feldspar ^p	6.79, 6.67	6.84
Dunaskin Glen			
DG-72	feldspar ^p	8.02, 8.02	8.13
DG-75	feldspar ^p	8.55, 8.41	8.59
Elie Ness			
END-1	feldspar ^p	9.10, 9.20	9.26
Z-1	zircon (1)	4.74	4.74
Z-2	zircon (1)	4.80	4.80
Z-3	zircon (2)	4.75	4.75
Z-4	zircon (2)	5.03	5.03
Z-5	zircon (4)	4.49	4.49
Z-6	zircon (1)	4.89	4.89
Z-7	zircon (1)	4.78	4.78
Fife			
PEP-10	biotite	5.30	5.18
Holmbyre			
HB-80	feldspar ^p	7.97, 8.04	8.11
Loch Roag			
LR core	corundum	4.84	4.84
LR rim	corundum	5.25	5.25
LR-9	feldspar ^p	6.65, 6.86	6.86
LR-182	biotite	5.51, 5.22	5.24
LR-250	corundum	4.65, 4.65	4.65
LR-290	corundum	4.83, 4.84	4.83
LR-299	biotite	5.54, 5.46	5.39

(1), (2), number of individual zircons analysed together; ^psample analysed as powder using airlock sample chamber; VSMOW values are normalized to UWG-2 standard (see Valley *et al.*, 1995).

DISCUSSION

Corundum-bearing parageneses

Coenraads *et al.* (1990) listed numerous localities worldwide where sapphire occurs in volcanic terrains. Syn-genetic inclusions (e.g. U-pyrochlore, thorite and columbite), as well as CO₂-filled inclusions, indicate that

the sapphires grew in environments rich in incompatible elements and volatiles. Dating the zircons in the sapphires showed them to be neo-contemporaneous with the basalt magmatism. The 'growth-zoning', CO₂-rich fluid inclusions, and high inclusion homogenization temperatures (>650°C) in sapphires from Queensland led Stephenson (1976) and Irving (1986) to infer high tem-

peratures and high pressures for their origin. Coenraads *et al.* (1990) concluded that the sapphires grew from highly evolved magmas in the deep crust or upper mantle. Guo *et al.* (1996b) concurred that the sapphires grew from highly fractionated silicate-rich melts but proposed a mid-crustal provenance. Sutherland *et al.* (1998), however, argued for a lithospheric mantle origin.

Observations on the Loch Roag and Burn-between-the-Laws corundums demonstrate clearly that they grew in dynamic environments that gave rise to complex oscillatory zoning and episodic resorption. Rhythmic growth zoning in zircons from Elie Ness suggests fluctuations in REE, Th and U content of the parent melt (Hinton & Upton, 1991). Together with the oxygen isotope data and the association with geochemically extreme mineral phases, the evidence denies a meta-sedimentary origin for the peraluminous xenoliths, as has been proposed for some kimberlite xenolith suites (e.g. Mazzone & Haggerty, 1989). The peraluminous trachytic melts from which the Scottish corundum syenite xenoliths are inferred to have crystallized are likely to have had SiO₂ contents in the region of 60%, total alkalis approximating 10% and Al₂O₃ contents probably in excess of 20%.

Whereas xenolith-megacryst studies are normally handicapped by the inability to observe 'field relationships', occasional tectonic slices of uplifted mantle may provide pertinent information. Possibly an analogy to the relationships under discussion is provided by an occurrence of 'hornblende peridotite' in Plumas County, California, which is cut by a 5 m dyke of feldspathic rock ('plumasite') comprising 83.6% oligoclase and 16.4% pale blue-violet corundum (Barlow, 1915). The modal proportions are very similar to those of the anorthoclase-corundum xenolith (BBL24). The half-metre thick zircon syenite pegmatitic dykes in the (mantle tectonite) phlogopite peridotites of the Finero mafic-ultramafic complex in the Ivrea Zone of the Alps (Stahle *et al.*, 1990) may also be analogous to the megacryst source rocks. These dykes have high Nb, Th, U and LREE, and are inferred to have crystallized from mantle-derived volatile-rich partial melts (Stahle *et al.*, 1990). In the same region an REE-rich alvikite carbonatite occurs containing inclusions of alkali feldspars and syenitic metasomites.

Subdivision of the assemblages and inferences concerning parent melts

It is clear that large variations exist in the trace element chemistry of individual feldspars and this must reflect differences in the chemistry of the melt from which they formed, the trace element partitioning related to their major element chemistry, or temperature-pressure considerations. Thus although, in the extreme cases, there is a difference of a factor of 1000 in the La content

between individual feldspars, observed relationships within each group suggest that a factor of 5–10 may be attributed to partitioning changes related to CaO content. It is unlikely that the remaining variation of ~200 in the La content for feldspars with similar CaO content can be attributed to either changes in melt major element chemistry or *P*, *T* conditions and must reflect variations in the REE content of the melt. The trace element subdivision of the feldspars referred to above can be used to subdivide the megacryst assemblages as a whole into three groups.

Group 1

The majority of the Group 1 samples are essentially monomineralic anorthoclases with CaO contents of <0.8%. They have moderate Sr and Ba contents and calculated melt compositions of ~100 ppm Sr and 250–700 ppm Ba (see Appendix for details of partition coefficients used). Although the REE abundances are 10–20 times lower than in Group 2 (see below and Fig. 10) the similarity of LREE patterns in the feldspars (Fig. 4) suggests comparable LREE–HREE values in the melt.

Group 2

These feldspars are associated with clinopyroxene and/or apatite and generally have higher CaO contents (1.4–3 wt %). The coexisting melts must have been enriched in Sr (150–300 ppm) and highly enriched in Ba (900–1800 ppm). Overall, the melts calculated using clinopyroxene and apatite (Fig. 10) give similar patterns of LREE enrichment (La/Yb 40–80) and flat, to gently sloping, HREE patterns (see Appendix for details of partition coefficients used). Whereas no Eu anomaly is observed in the calculated melt pattern, there is a significant positive Eu anomaly in the feldspar; the melt must have been sufficiently oxidizing to limit the abundance of Eu²⁺. Although the overall degree of REE enrichment calculated is dependent on the choice of partition coefficient for pyroxene, it is within a factor of two of the calculated REE budget for GR117 (based on observed mineral proportions). The Zr and Nb contents of the pyroxenes are consistent with relatively high whole-rock Zr and Nb contents of 100–500 ppm.

Group 3

This comprises feldspars coexisting with corundum as well as with Nb–Ti–Th-rich oxide phases and zircon. Other silicates and apatite are scarce or absent. The feldspars have low Sr and Ba (with melt values estimated 4–30 ppm and 7–100 ppm, respectively) but high LREE. The La/Ce ratio is significantly lower than in feldspars of the other groups, consistent with the depletion of La relative to Ce observed in the REE-rich phases (Fig. 9). Estimation of the original melt chemistry is difficult given

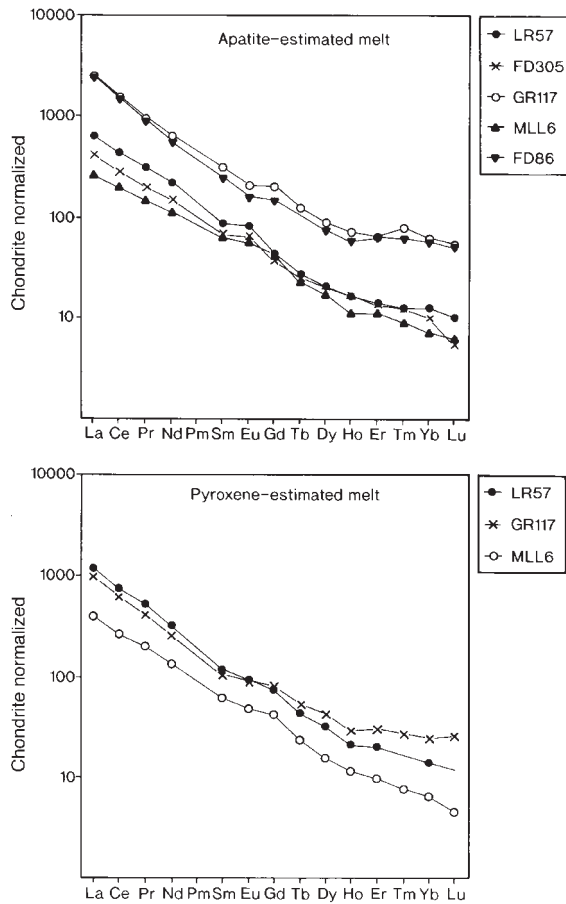


Fig. 10. Estimated chondrite-normalized REE patterns for melts equilibrated with a selection of apatites and clinopyroxenes from the megacryst suites. Chondrite values for normalization from Anders & Grevesse (1989).

the concentration of REE into minor phases but all evidence suggests that the melt must have been strongly enriched in the REE (possibly higher than $4000 \times C1$ chondrites). The depletion of La relative to Ce suggests that the melt had a flatter overall pattern than that estimated for the other two groups. Although more reducing conditions are suggested by the strong negative Eu anomalies observed in the oxide phases and zircon (Hinton & Upton, 1991), there may be sufficient Eu within the feldspar to permit the melt to have no Eu anomaly. However, a melt with a negative Eu anomaly is more likely, given that both Sr and Ba are depleted and the melt is depleted in Ca and Mg. The differences between Group 2 and Group 3 feldspars are reflected in the coexisting zircons. The inferred melt chemistry for RSM2 [a companion sample to RSM1 (Hinton & Upton, 1991)] has a distinct negative Eu anomaly and high REE abundance, whereas EN2B has no Eu anomaly and variable, but lower, REE content.

The petrography of xenolith BBL24 shows that it had a history in which corundum growth in a changing environment was terminated by an episode of dissolution and anorthoclase crystallization. Subsequent partial alteration of the anorthoclase to a more potassic feldspar was followed by introduction of two generations of calcite veins. Whereas the second of these may be attributed to late-stage, low-temperature hydrothermal processes, the first generation is (as has been noted above) associated with metasomatic effects of the feldspar side-walls. It would appear that fluids, introduced at an early stage after crystallization of the anorthoclase–corundum rock, affected the feldspar, leaching Na and adding K (plus Rb and Cs). Subsequently, the first-generation calcite veins appear to have been generated by carbonate-rich fluids which were responsible for the HFSE, Ba, Sr, Li and B (as well as Mg, Mn and Fe) metasomatism.

Possible role of carbonatite melts

Long *et al.* (1994) presented data on the Loch Roag megacrysts and pointed out that, as some of the pyroxenes and micas have *mg*-numbers too high to have been in equilibrium with a trachytic melt (*pace* Aspen *et al.*, 1990) and that they equilibrated with a more basic melt, the Loch Roag megacrysts must be polygenetic. Considering coexisting carbonatite–silicate melts, Long *et al.* (1994) noted [from consideration of Hamilton *et al.* (1989)], that enrichment of the carbonate fraction in REE is favoured by high pressures and increased polymerization of the silicate melt. In the shallow upper mantle, the REE would preferentially concentrate (by a factor of 10 or more) into the carbonatite fraction of any conjugate melt pair. Long *et al.* (1994) commented on the similarity between the parental melts inferred for the Loch Roag megacrysts and carbonatite melts, and noted that the enrichment in Ba, K, Nb, LREE and Sr characterizing the pyroxenites points to possible influx of carbonatitic melts that may have been genetically related to the basaltic magmatism that hosted the xenoliths and megacrysts. In contrast to the on-craton Loch Roag situation, however, Long *et al.* (1994) inferred that the melts which coexisted with the Scottish off-craton megacrysts were not so markedly enriched in LREE. Whereas this may generally be true, our data show that the extreme LREE enrichment exhibited by the feldspars associated with the Loch Roag corundums is actually surpassed by those in the corundum-bearing xenoliths at Ruddon's Point and Burn-between-the-Laws in SE Scotland, remote from the craton.

According to Guo *et al.* (1996b), the compositions of columbite and U-pyrochlore in basalt-hosted corundum megacrysts suggest a source of carbonatitic character. Those workers concluded that the corundum genesis

involved interaction of carbonatitic magma with alkali syenite or granite pegmatite compositions (magmas or rocks) at mid-crustal levels and temperatures of 400°C. However, although conceding that the evidence from these Scottish assemblages (particularly, but not exclusively, the peraluminous cases), supports the participation of carbonatitic melts, our data indicate shallow mantle sources at temperatures in excess of 700°C (Aspen *et al.*, 1990), in agreement with the corundum crystallization temperatures of 685–900°C proposed by Sutherland *et al.* (1998).

A carbonatite association is consistent with the low content of divalent cations, including Mg, Sr, Ba and probably, Eu. Ca may be increased because the overwhelming concentration of Ca is such that even high partitioning of Ca into the melt will lead to a relatively high content of Ca in the silicate. The REE may be similarly enriched but with a noticeable change in the La/Ce ratio in the most REE-rich cases consistent with high La vs Ce fractionation into the carbonatite. A carbonatite would exclude Al, Ti, Zr and Th, increasing the elements in the silicate–oxide phases. Hf is taken into the silicate in preference to Zr (Fielding, 1992) providing a possible explanation of the high Hf content of the RSM1 zircons. Si, Nb and Ta will partition strongly into the silicate but this partitioning is less extreme than that for Al. U, P, together with Ba would preferentially stay in the carbonatite, thus offering possible explanation for the preponderance of phases with relatively high Th/U values. However, if carbonatite melts were involved in the genesis of the megacrysts then carbonate was subsequently wholly lost to the system.

Several workers (e.g. Meen, 1987; Green & Wallace, 1988; Wallace & Green, 1988; Lee & Wyllie, 1998) have concluded that reaction between carbonated nephelinite or carbonatite and mantle harzburgite or lherzolite produces clinopyroxene-rich wall rocks (wehrlite or olivine pyroxenite). Lee & Wyllie (1998) noted that, at depths <70 km, wehrlite can coexist with carbonatite melts relatively enriched in Ca/Mg. Long *et al.* (1994) commented on the similarity between the parental melts inferred for the Loch Roag megacrysts and carbonatite melts, and noted that the enrichment in Ba, K, Nb, LREE and Sr characterizing the pyroxenites points to possible influx of carbonatitic melts. CO₂ degassing of the mantle was held by Menzies & Wass (1983) to be responsible for migration of REE-rich fluids and localized transformation of lherzolite to pyroxenites veined by apatite ± kaersutite ± biotite ± diopside. More recently, Baker *et al.* (1998) concluded that amphibole ± apatite-bearing lherzolite xenoliths from Yemen have characteristics consistent with enrichment of shallow mantle by carbonatite melts and hydrous fluids.

Relationship to glasses in mantle xenoliths

The paragenesis of the megacryst associations may have some relationship to the formation of some of the salic and alkalic glass patches reported from mantle xenoliths. Compositions of such glasses vary widely [see Chazot *et al.* (1996) and references therein], with SiO₂ 52–65%, Al₂O₃ 18–23%, Na₂O 3–10% and K₂O 0.3–2.3%. Although the origins of these glasses may be diverse, Schiano *et al.* (1994) and Eiler *et al.* (1993) concluded that some glass inclusions represent small amounts of metasomatic melts with compositions dramatically different from those of the host magmas, originating at depth as part of an exotic migrating phase in the lithosphere. Draper & Green (1997) proposed a two-stage model to account for the Si–Al–alkali-rich melts corresponding to mantle xenolith glasses. Stage 1 involves enrichment of the mantle (at ~45–90 km depth) in low-melting components by percolating alkali mafic liquids whereas Stage 2 involves subsequent low-degree partial melting to yield the liquids ultimately trapped as xenolith glasses. The calculated REE patterns from the apatite and pyroxene megacrysts (Fig. 10) are comparable with those described by Schiano *et al.* (1994) for mantle glasses. A chondrite-normalized La concentration of 200–400 falls steadily to ~10–20 at Yb and there is no Eu anomaly. Although the major element chemistry of the glasses is similar to the likely composition of the melts from which the pyroxene megacrysts crystallized, the CaO content is, however, too high for many of the samples studied.

Salic melts in the shallow mantle

Evidence that alkaline salic magmas can be produced within the sub-continental lithospheric mantle was reviewed by Aspen *et al.* (1990), who deduced that volatile fluxes interacting with the lithospheric mantle led to small-fraction melts from which the highly evolved, feldspathic rocks crystallized. That these melts were trachytic rather than benmoreitic (see Guo *et al.*, 1996a) is evident from the high Fe/Mg nature of associated ferromagnesian silicate and oxide phases and the high (Na + K)/Ca of most of the feldspars. These melts appear to have had alkali:silica proportions buffered so that neither silica-oversaturated nor feldspathoidal compositions have yet been encountered. The most extremely fractionated (peraluminous) melts yielded alkali feldspar rocks with accompanying oxides but apparently lacking ferromagnesian silicates.

A petrogenetic problem arises in that the megacrysts and xenoliths studied indicate that the parental melts were, in some cases, peraluminous. The concept of melts yielding corundum being peralkaline (see Guo *et al.*, 1996b) is clearly untenable. Normal fractional crystallization processes will not give rise to peraluminous

residues [other than in calc-alkaline environments; see Cawthorn *et al.* (1976)]. Accordingly, if assimilation of aluminous (metasedimentary) material is excluded, the peraluminous condition may have been brought about by alkali loss. Whereas the melts parental to the B-group megacrysts must all have been relatively highly evolved [low *mg*-number, high $(\text{Na}_2\text{O} + \text{K}_2\text{O})/\text{CaO}$, high Zr, P, REE], those from which the corundum-bearing assemblages formed were the most extreme (see Guo *et al.*, 1996*b*) and their inferred very high LREE, Nb, Ta, U and Th concentrations suggest the involvement of carbonatite. The calcite veining (e.g. in xenolith BBL24), as well as the remarkable carbonate-filled tubules described from some anorthoclase megacrysts (Aspen *et al.*, 1990) may point to the separation of a conjugate carbonatite melt from a carbonate-rich trachyte magma. If so, alkali loss leaving a peraluminous residuum may have been brought about by such a fugitive carbonatite melt. Sutherland *et al.* (1999) maintained that melts generated from amphibole-bearing mantle sources can produce corundum in Nb- and Ta-enriched residual liquids.

SUMMARY

We conclude that the Scottish lithospheric peridotites were locally metasomatized by alkali-rich carbonatitic melts with production of wehrlites and assorted amphibole \pm biotite pyroxenites. Within these metasomatized products, carbonated trachytic melts (approximating to the sanidine–salite cotectic) were generated, although the precise manner of their formation remains obscure. The lack of more primitive assemblages suggests that these are not crystal fractionation residues [and specifically not evolved derivatives of basaltic magma as suggested by Guo *et al.* (1996*a*)]. Conversely, they may represent small-fraction melts produced from metasomatized mantle, as proposed by Draper & Green (1997) for mantle xenolith glasses. Similar conclusions with respect to the Australian corundum–zircon, etc. associations, namely, that they crystallized from felsic melts derived from partial melting of amphibole- or biotite-bearing metasomatized mantle, were presented by Barron *et al.* (1996), Sutherland (1996) and Sutherland *et al.* (1998).

In the Scottish lithospheric mantle these felsic melts crystallized to syenites that were commonly pegmatitic (grain-size up to ~20 cm). In the most extremely evolved cases, peraluminous compositions were attained, possibly as a result of alkali loss in a conjugate carbonatitic fraction with crystallization of corundum-bearing syenites. Late-stage fluid–rock interactions (between crystalline rock and fugitive carbonatite fluids?) are evidenced in many of the alkali feldspathic xenoliths. Composite xenoliths

from Loch Roag and Gribun provide evidence that the megacryst melts were hosted by biotite pyroxenites and pargasite pyroxenites, although at Fidra the felsic melts were associated with anhydrous wehrlite–clinopyroxenite host rocks. The general similarity of the megacryst assemblages across all five of the major tectonic units of Scotland (Fig. 1) suggests that the processes involved were comparable beneath more than 300 km of terrain. We conclude that the Scottish megacryst suites come from geochemically enriched veins within heterogeneous, metasomatized shallow mantle, generated in response to complex, late Palaeozoic melting episodes.

ACKNOWLEDGEMENTS

We are grateful to P. Hill, S. Cairns and J. Craven for assistance with regard to electron microprobe and ion microprobe analyses, to M. Spicuzza for stable isotope analyses, and to P. Ainsworth (Glasgow University) for SEM analyses. The Edinburgh ion microprobe is supported by NERC Science Programmes Directorate and research grants. We also thank R. Macdonald, S. Y. O'Reilly, M. A. Menzies and M. Wilson for constructive criticism.

REFERENCES

- Anders, E. & Grevesse, N. (1989). Abundances of the elements: meteoritic and solar. *Geochimica et Cosmochimica Acta* **53**, 197–214.
- Aspen, P., Upton, B. G. J. & Dickin, A. P. (1990). Anorthoclase, sanidine and associated megacrysts in Scottish alkali basalts: high-pressure syenitic debris from upper mantle sources? *European Journal of Mineralogy* **2**, 503–517.
- Baker, J., Chazot, G., Menzies, M. & Thirlwall, M. (1998). Metasomatism of the shallow mantle beneath Yemen by the Afar plume—implications for mantle plumes, flood volcanism, and intraplate volcanism. *Geology* **26**, 431–434.
- Barlow, A. E. (1915). Corundum, its occurrence, distribution, exploitation and uses. *Canada Department of Mines, Geological Survey Memoir* **57**, 377.
- Barron, B. J., Robertson, A. D. & Sutherland, F. L. (1996). Olivine 'leucitites', their xenolith and megacryst suites, Hoskings Peaks, north Queensland. *Australian Journal of Earth Sciences* **43**, 231–244.
- Barton, M., Varekamp, J. C. & Van Bergen, M. J. (1982). Complex zoning of clinopyroxenes in the lavas of Vulcini, Latium: evidence of magma mixing. *Journal of Volcanology and Geothermal Research* **14**, 361–388.
- Blundy, J. D. & Wood, B. J. (1991). Crystal-chemical controls on the partitioning of Sr and Ba between plagioclase feldspar, silicate melts, and hydrothermal solutions. *Geochimica et Cosmochimica Acta* **55**, 193–209.
- Brooks, C. K. & Printzlau, I. (1978). Magma mixing in mafic alkaline volcanic rocks: the evidence from relict phenocryst phases and other inclusions. *Journal of Volcanology and Geothermal Research* **4**, 315–331.
- Cawthorn, R. G., Strong, D. F. & Brown, P. A. (1976). Origin of corundum-normative intrusive and extrusive magmas. *Nature* **259**, 102–104.

- Chapman, N. A. (1976). Inclusions and megacrysts from undersaturated tuffs and basanites, E. Fife, Scotland. *Journal of Petrology* **17**, 472–498.
- Chazot, G., Menzies, M. & Harte, B. (1996). Silicate glasses in spinel lherzolites from Yemen: origin and chemical composition. *Chemical Geology (Isotope Geoscience)* **134**, 159–179.
- Coenraads, R. R., Sutherland, F. L. & Kinny, P. (1990). The origin of sapphires: U–Pb dating of zircon inclusions sheds new light. *Mineralogical Magazine* **54**, 113–122.
- Coltorti, M., Bonadiman, C., Hinton, R. W., Siena, F. & Upton, B. G. J. (1999). Carbonatite metasomatism of the oceanic upper mantle: evidence from clinopyroxenes and glasses in ultramafic xenoliths of Grande Comore, Indian Ocean. *Journal of Petrology* **40**, 133–165.
- Colvine, R. J. L. (1968). Pyrope from Fife. *Scottish Journal of Geology* **4**, 283–286.
- De St Jorre, L. & Smith, D. G. W. (1988). Cathodoluminescent Ga-enriched feldspars from the Thor Lake rare-metal deposits, Northwest Territories. *Canadian Mineralogist* **26**, 301–308.
- Donaldson, C. H. (1984). Kinetics of pyrope megacryst reaction in ascending basaltic magma—relevance to high-pressure magmatic crystallisation at Elie Ness, East Fife. *Geological Magazine* **21**, 615–620.
- Draper, D. S. & Green, T. H. (1997). *P–T* phase relations of silicic, alkaline, aluminous xenolith glasses under anhydrous and C–O–H fluid-saturated conditions. *Journal of Petrology* **38**, 1187–1224.
- Duda, A. & Schmincke, H.-U. (1985). Polybaric differentiation of alkali basaltic magmas: evidence from green-core clinopyroxenes (Eifel, FRG). *Contributions to Mineralogy and Petrology* **91**, 340–353.
- Eiler, J. M., Valley, J. W. & Baumgartner, L. P. (1993). A new look at stable isotope thermometry. *Geochimica et Cosmochimica Acta* **57**, 2571–2583.
- Ferguson, J. & Fielding, P. E. (1971). The origin of the colours of yellow, green and blue sapphires. *Chemical Physics Letters* **10**, 262–265.
- Fielding, K. (1992). Element partitioning between coexisting carbonate and silicate liquids. Ph.D. Thesis, University of Edinburgh.
- Frondel, C. (1954). Commercial synthesis of star sapphires and star rubies. *Transactions of the American Institute of Mining and Metallurgy* **6**(1), 78–80.
- Fujimaki, H. (1986). Partition coefficients of Hf, Zr, and REE between zircon, apatite and liquid. *Contributions to Mineralogy and Petrology* **94**, 42–45.
- Ghiorso, S. M. & Sack, O. R. (1991). Fe–Ti oxide geothermometry: thermodynamic formulation and estimation of intensive variables in silicic magmas. *Contributions to Mineralogy and Petrology* **108**, 485–510.
- Gilliam, C. E. & Valley, J. W. (1997). Low $\delta^{18}\text{O}$ magma, Isle of Skye, Scotland: evidence from zircons. *Geochimica et Cosmochimica Acta* **61**, 4975–4981.
- Green, D. H. (1994). Experimental studies of trace-element partitioning applicable to igneous petrogenesis—Sedona 16 years later. *Chemical Geology* **117**, 1–36.
- Green, D. H. & Wallace, M. E. (1988). Mantle metasomatism by ephemeral carbonatite melts. *Nature* **336**, 459–462.
- Green, T. H. & Pearson, N. J. (1985). Rare earth element partitioning between clinopyroxene and silicate liquid at moderate to high pressure. *Contributions to Mineralogy and Petrology* **91**, 24–36.
- Guo, J. F., Green, J. F. & O'Reilly, S. Y. (1996a). Ba partitioning and the origin of anorthoclase megacrysts in basaltic rocks. *Mineralogical Magazine* **56**, 101–107.
- Guo, J., O'Reilly, S. Y. & Griffin, W. L. (1996b). Corundum from basaltic terrains: a mineral inclusion approach to the enigma. *Contributions to Mineralogy and Petrology* **122**, 368–386.
- Hamilton, D. L., Bedson, P. & Esson, J. (1989). The behaviour of trace elements in the evolution of carbonatites. In: Bell, K. (ed.) *Carbonatites*. London: Unwin Hyman, pp. 405–427.
- Hinton, R. W. & Upton, B. G. J. (1991). The chemistry of zircons and coexisting phases from alkali basalt xenoliths and a syenite. *Geochimica et Cosmochimica Acta* **55**, 3287–3302.
- Hunter, R. H. & Upton, B. G. J. (1987). The British Isles—a Palaeozoic mantle sample. In: Nixon, P. H. (ed.) *Mantle Xenoliths*. New York: John Wiley, pp. 107–118.
- Hunter, R. H., Upton, B. G. J. & Aspen, P. (1984). Meta-igneous granulite and ultramafic xenoliths from basalts of the Midland Valley of Scotland: petrology and mineralogy of the lower crust and upper mantle. *Transactions of the Royal Society of Edinburgh, Earth Science* **75**, 75–84.
- Irving, A. J. (1980). Petrology and geochemistry of composite ultramafic xenoliths in alkalic basalts and implications for magmatic processes within the upper mantle. *American Journal of Science* **280-A**, 389–426.
- Irving, A. J. (1984). Polybaric mixing and fractionation of alkalic magmas: evidence from megacryst suites. *EOS Transactions, American Geophysical Union* **65**, 1153.
- Irving, A. J. (1986). Polybaric magma mixing in alkali basalts and kimberlites: evidence from corundum, zircon and ilmenite megacrysts. *4th International Kimberlite Conference, Perth, 1986, Geological Society of Australia Abstract Series* **16**, 262–264.
- Irving, A. J. & Frey, F. A. (1984). Trace element abundances in megacrysts and their host basalts: constraints on partition coefficients and megacryst genesis. *Geochimica et Cosmochimica Acta* **48**, 1201–1221.
- Kotomin, E. A., Popov, A. I. & Stashans, A. (1994). A novel model for F^+ – F photoconversion in corundum crystals. *Journal of Physics and Condensed Matter* **6**, L569–L573.
- Laud, K. R., Gibbons, E. F., Tien, T. Y. & Stadler, H. L. (1971). Cathodoluminescence of Ce^{3+} and Eu^{2+} activated alkaline earth feldspars. *Journal of the Electrochemical Society: Solid State Science* **118**, 918–923.
- Lee, W.-J. & Wyllie, P. J. (1998). Petrogenesis of carbonatitic magmas from mantle to crust, constrained by the system $\text{CaO}-(\text{MgO} + \text{FeO}^*)-(\text{Na}_2\text{O} + \text{K}_2\text{O})-(\text{SiO}_2 + \text{Al}_2\text{O}_3 + \text{TiO}_2)-\text{CO}_2$. *Journal of Petrology* **39**, 495–518.
- Long, A. M., Menzies, M. A., Thirlwall, M. F., Upton, B. G. J. & Aspen, P. (1994). Carbonatite–mantle interaction: a possible origin for megacryst/xenolith suites in Scotland. In: Meyer, H. O. A. & Leonardos, O. H. (eds) *Kimberlites, Related Rocks and Xenoliths. 1, International Kimberlite Conference, Brazil 1991*, pp. 467–477.
- Mariano, A. N. (1988). Some further applications of cathodoluminescence. In: Marshall, D. J. (ed.) *Cathodoluminescence of Geological Materials*. New York: Unwin Hyman, pp. 94–123.
- Mason, R. A., Smith, J. V., Dawson, J. B. & Treves, S. B. (1982). A reconnaissance of trace elements in anorthoclase megacrysts. *Mineralogical Magazine* **46**, 7–11.
- Matson, S. M. & Rossman, G. R. (1988). Fe^{2+} – Ti^{4+} charge transfer in stoichiometric Fe^{2+} , Ti^{4+} minerals. *Physics and Chemistry of Minerals* **16**, 76–82.
- Mazzone, P. & Haggerty, S. E. (1989). Peraluminous xenoliths in kimberlite: metamorphosed restites produced by partial melting of pelites. *Geochimica et Cosmochimica Acta* **53**, 1551–1561.
- Meen, J. K. (1987). Mantle metasomatism and carbonatites: an experimental study of a complex relationship. *Geological Society of America, Special Paper* **215**, 91–100.
- Menzies, M. A. & Halliday, A. N. (1988). Lithospheric mantle domains beneath the Archean and Proterozoic crust of Scotland. *Journal of Petrology, Special Lithosphere Issue* 275–302.
- Menzies, M. A. & Wass, S. Y. (1983). CO_2 - and LREE-rich mantle below eastern Australia: a REE and isotopic study of alkaline magmas and apatite-rich mantle xenoliths from the Southern Highlands Province, Australia. *Earth and Planetary Science Letters* **65**, 287–302.

- Monani, S. B. & Valley, J. W. (1998). Zircon record low $\delta^{18}\text{O}$ magmas: Skye and Arran, Scotland. Abstract. Geological Society of America, Annual Meeting.
- Muan, A. & Gee, C. L. (1955). Phase equilibrium studies in the system iron oxide– Al_2O_3 in air and at 1 atm. O_2 pressure. *Journal of the American Ceramic Society* **39**, 207.
- Reisfeld, R., Eyal, M. & Jorgensen, C. K. (1987). Unusual luminescence of Ti (III) in aluminium oxide. *Chimia* **41**, 117–119.
- Schiano, P., Clochiatti, R. & Shimizu, N. (1994). Melt inclusions trapped in mantle minerals: a clue to identifying metasomatic agents in the upper mantle beneath continental and oceanic intraplate regions. *Mineralogical Magazine* **58A**, *V.M. Goldschmidt Conference*, 807–808.
- Schnetzler, C. C. & Philpotts, J. A. (1970). Partition coefficients of rare-earth elements between igneous matrix material and rock-forming mineral phenocrysts. II. *Geochimica et Cosmochimica Acta* **34**, 331–340.
- Sheikh, A. B. & Irvine, J. T. S. (1993). Phase formation and electrical transport properties in the corundum (Ti_2O_3)–ilmenite (MgTiO_3) system. *Journal of Solid State Chemistry* **103**, 30–37.
- Spicuzza, M. J., Valley, J. W. & McConnell, V. S. (1998). Oxygen isotope analysis of whole rock via laser fluorination: an air-lock approach. Abstract. Geological Society of America, Annual Meeting.
- Stahle, V., Frenzel, G., Kober, B., Michard, A., Puchelt, H. & Schneider, W. (1990). Zircon syenite pegmatites in the Finero peridotite (Ivrea Zone): evidence for a syenite from a mantle source. *Earth and Planetary Science Letters* **101**, 196–205.
- Stephenson, P. J. (1976). Sapphire and zircon in some basaltic rocks from Queensland, Australia. *Abstracts of the 25th International Geological Congress, Sydney* **2**, 602–603.
- Sutherland, F. L. (1996). Alkaline rocks and gemstones, Australia: a review and synthesis. *Australian Journal of Earth Sciences* **43**, 323–343.
- Sutherland, F. L., Hoskin, P. W. O., Fanning, C. M. & Coenraads, R. R. (1998). Models of corundum origin from alkali basaltic terrains: a reappraisal. *Contributions to Mineralogy and Petrology* **133**, 356–372.
- Tait, A. S. (1959). Asterism in corundum. *Journal of Gemmology* **5**, 65–72.
- Thompson, R. N. (1974). Some high-pressure pyroxenes. *Mineralogical Magazine* **39**, 768–787.
- Upton, B. G. J., Aspen, P. & Chapman, N. A. (1983). The upper mantle and deep crust beneath the British Isles: evidence from inclusion suites in volcanic rocks. *Journal of the Geological Society, London* **140**, 105–122.
- Upton, B. G. J., Aspen, P. & Hunter, R. H. (1984). Xenoliths and their implications for the deep geology of the Midland Valley of Scotland and adjacent regions. *Transactions of the Royal Society of Edinburgh, Earth Sciences* **75**, 65–70.
- Upton, B. G. J., Aspen, P., Rex, D. C., Melcher, F. & Kinny, P. (1998). Lower crustal and possible shallow mantle samples from beneath the Hebrides: evidence from a xenolithic dyke at Gribun, western Mull. *Journal of the Geological Society, London* **155**, 813–828.
- Valley, J. W., Kitchen, N., Kohn, M. J., Niendorf, C. R. & Spicuzza, M. J. (1995). UWG-2, a garnet standard for oxygen isotope ratios: strategies for high precision and accuracy with laser heating. *Geochimica et Cosmochimica Acta* **59**, 5223–5231.
- Valley, J. W., Kinny, P. D., Schulze, D. J. & Spicuzza, M. J. (1998). Zircon megacrysts from kimberlite: oxygen isotope variability among mantle melts. *Contributions to Mineralogy and Petrology* **133**, 1–11.
- Walker, G. (1985). Mineralogical applications of luminescence techniques. In: Berry, F. L. & Vaughan, D. J. (eds) *Chemical Bonding and Spectroscopy in Mineral Chemistry*. London: Chapman and Hall, pp. 103–140.
- Wallace, M. E. & Green, D. H. (1988). An experimental determination of primary carbonatite magma composition. *Nature* **335**, 343–346.

APPENDIX

The partition coefficients for Sr and Ba between feldspar and melt, based on Blundy & Wood (1991), for the compositions encountered in this work would be close to 1.1 and 1.9, respectively, assuming An 0.1 and 950°C. Variations as a result of the variable CaO content are not likely to exceed 30%. The partitioning of the REE between feldspar and melt has not been studied in enough detail to give close estimates of the melt composition but the D_{La} values are likely to fall in the range of 0.02–0.5 for the more calcic feldspars [see, e.g. Schnetzler & Philpotts (1970)]. Calculated melts should therefore have chondrite-normalized La contents of between 100 and 2000. However, given that alkali feldspar partition coefficients are often 5–8 times lower than those of coexisting plagioclases, the partition coefficients for the CaO-poor compositions may be lower than these values (and calculated melts have higher REE contents). The partitioning of trace elements between clinopyroxene and melt has been studied in more detail [see Green (1994) for compilation] and, in general, the partition coefficients for REE increase with increasing pressure and SiO_2 content but decrease with increasing temperature. The partitioning at 950°C, 10 kbar and SiO_2 of 60% (Green & Pearson, 1985) would give a partition coefficient of approximately three for Ho. In contrast, calculated clinopyroxene D values for coexisting clinopyroxene (which should have equilibrated at about this temperature, pressure and composition) given by Coltorti *et al.* (1999) fall close to, or just below, unity. Similar data from Chazot *et al.* (1996) give partition coefficients for clinopyroxene coexisting with apatite, amphibole and an alkali-rich glass which fall at the extreme end of coefficients determined from experimental and natural samples (partitioning for HREE ~ 1.5). Apatite–melt partition coefficients, like clinopyroxene–melt values, increase with increasing SiO_2 and decreasing temperature but are largely independent of pressure (Green, 1994). Ho partition coefficients as high as 30 can be expected for granites but only three for tholeiitic melts. Measured partitioning between these phases gives Ho apatite/clinopyroxene ratios of 4–6 (Chazot *et al.*, 1996) and 4, 5 and 14 (this work). This constrains the apatite–clinopyroxene partition coefficients for Ho to be close to six. Melt compositions have been calculated using a combination of $D_{\text{cpx-melt}}$ of BA5 (Chazot *et al.*, 1996) and $D_{\text{apatite-melt}}$ [Fujimaki (1986), scaled down to give a apatite–clinopyroxene factor of six]. Although, given the above considerations, it is expected that the calculated melt concentrations represent maximum values, calculation of the total REE budget for GR117 gives La close to 500 times chondritic concentrations, similar to that calculated for apatite and a factor of two lower than that calculated using clinopyroxene.